TIME OF ARRIVAL ESTIMATION WITH MUSIC UNDER IMPULSIVE NOISE

by

İSA HACIOĞLU

B.S., Electronics and Telecommunications Engineering

Yıldız Technical University

2001

Submitted to the Institute for Graduate Studies in
Science and Engineering in partial fulfillment of
the requirements for the degree of
Master of Science

Graduate Program in Electrical and Electronics Engineering

Boğaziçi University

2005

ACKNOWLEDGEMENTS

First of all, I would like to thank to my supervisors Prof. Emin Anarım and Prof. Hakan Deliç for their invaluable help and encouragement. This thesis could not be accomplished without their support.

I am grateful to Assist. Prof. Kerem Harmancı for not only his help but also his friendship. Whenever I faced problems during the preparation of this thesis, He helped me without hesitation.

I am also thankful to the members of the committee, namely, Prof. Cem Ersoy, and Assist. Prof. Mutlu Koca.

Lastly, I could succeed simply nothing without my family. The last sentence is for my father, the most valuable person I ever had in my life. Although He is not with me anymore, I will always feel his support and work hard to do my best for him.

ABSTRACT

TIME OF ARRIVAL ESTIMATION WITH MUSIC UNDER IMPULSIVE NOISE

With the emergence of micro and nano technologies, the context-aware wireless communications applications have been spreading. Especially, location-awareness has gained significance recently.

The TOA estimation have been chosen by many wireless communications technologies such as GSM, and GPS as a ranging metric for locating their subscribers. Once the TOA is estimated accurately, the distance between the transmitter and receiver is readily obtained. The TOA is estimated from the first arriving signal component. If the first multipath component is not detectable, the accuracy of the localization scheme is threatened.

The environmental noise is another significant factor that affects the performance of the TOA estimator. Although most wireless communication researches assume that noise in the environment has Gaussian distribution, it has been shown that many real-world noise signals have impulsive nature which cannot be modelled by Gaussian distribution. Instead, the stable distributions are used to model impulsive signals.

The super-resolution FLOM-MUSIC method is proposed to obtain the delay characteristics of indoor channels under impulsive noise, and the performance comparison between the FLOM-MUSIC and the traditional SOS-MUSIC is done. The improved performance with FLOM-MUSIC TOA estimator under impulsive noise is shown via simulations.

ÖZET

DARBE ÖZELLİKLİ GÜRÜLTÜ ALTINDA MUSIC ALGORİTMASI İLE VARIŞ ZAMANININ KESTİRİLMESİ

Son yıllarda elektronik ve haberleşme alanlarındaki gelişmeler ve özellikle telsiz haberleşmenin inanılmaz bir şekilde yaygınlaşması, konum tespit sistemlerinin önemini ve onlara olan talebi arttırdı. Günümüzde GSM (Küresel Gezgin Haberleşme Sistemi) ve GPS (Küresel Konumlandırma Sistemi) teknolojileri en popüler konum bulma servis sağlayıcılarıdir. Bu ve benzeri birçok teknoloji, konumlandırma hizmetlerinde sinyalin uçuş süresinden faydalanmaktadır.

Öte yandan ortamdaki gürültünün istatistiksel modelinin de kestirilen konum bilgisinin doğruluğuna etkisi önemlidir. Uzun yıllar boyunca sinyal işleme uygulamalarında ortam gürültüsünün Gauss dağılımına sahip olduğu kabul edildi ve sinyal alıcı tasarımları bu kabule göre yapıldı. Ancak son yıllarda yapılan araştırmalarda birçok yapay gürültü kaynağının aslında Gauss modeline uymayan sinyaller yaydıkları ve Gauss dağılımına göre tasarlanan alıcıların bu tip ortamlarda kötü performans gösterdikleri ispatlanmıştır. Gauss dağılımına sahip olmayan bu sinyallerin darbe özellikli olduğu ve α- kararlı dağılım modeli ile temsil edilebileceği gösterilmiştir.

Bu çalışmanın konusu, darbe özellikli gürültülü iç ortamlarda radyo kanalının gecikme özelliklerinin tespit edilmesi yoluyla konumlandırma yapılmasıdir. Bu amaç için yüksek çözünürlük sağlayan MUSIC (Çoklu Sinyal Sınıflandırma) yöntemi kullanılmıştır. Yapılan benzetimlerle Gauss modeli ile tasarlanan alıcılar darbe özellikli gürültü altında düşük verimle çalışırken tezde önerilen yöntemin tatmin edici bir performans sunduğu gösterilmiştir.

TABLE OF CONTENTS

LIST OF FIGURES

LIST OF SYMBOLS/ABBREVIATIONS

A	Positive semi-definite symmetric matrix
a	Location parameter of a stable distribution
$\mathbf{C}$	FLOM-based covariation matrix
C^{FB}	FLOM-based covariance matrix with Forward-Backward improvement
C^{G}	FLOM-based covariance matrix with general improvement
$\mathbf{D}$	Diagonal matrix
f_s	Sampling Frequency
$F(x)$	Univariate α-stable distribution function
$f(x; \alpha, \beta)$	Probability density function of a standard stable random variable
Δf	Frequency sampling interval
$\mathbf{J}$	Signal eigenvectors
$\mathbf{K}$	Noise eigenvectors
M	The length of an observed data vector
N	The number of snapshots
p	The fractional lower order moment order
P	the number of multipaths
S	k-dimensional unit sphere
S_{MUSIC}	MUSIC pseudospectrum
sign	Signum function
T	Transpose operation
$\varphi(t)$	Characteristic function
W	Exchange matrix
α	Characteristic exponent
β	Symmetry parameter
γ	Dispersion

$\Gamma(\cdot)$	Gamma function
σ_τ	rms delay spread
Φ	Projection matrix of the noise subspace
τ_{max}	Maximum path delay
$\overline{\tau}$	Mean excess delay
$\hat{\tau}_0$	The estimate of the first arriving path
$\mu(\cdot)$	Finite Borel measure on S

AOA	Angle-of-Arrival
AR	AutoRegressive
ARMA	AutoRegressive Moving-Average
AWGN	Additive White Gaussian Noise
BPSK	Binary Phase Shift Keying
BTS	Base Transceivers
CRLB	Cramér-Rao Lower Bound
CW	Continuous Wave
DDP	Dominant Direct Path
DFT	Discrete Fourier Transform
DLOS	Direct Line-of-Sight
DSSS	Direct Sequence Spread Spectrum
E-OTD	Enhanced Observed Time Difference of Arrival
FCC	Federal Communications Commission
FIR	Finite Impulse Response
FLOM	Fractional Lower Order Moment
FLOS	Fractional Lower Order Statistics
GCC	Generalized Covariation Coefficient
GPS	Global Positioning Systems
GSM	Global Positioning Systems
GSNR	Generalized Signal-to-Noise Ratio
IFFT	Inverse Fast Fourier Transform
LOS	Line-of-Sight

MEO	Medium Earth Orbit
MEMS	Micro-Electro-Mechanical Systems
MS	Mobile Station
MSE	Mean-Squared-Error
MUSIC	MUltiple Signal ClassifICation
NDDP	Non-Dominant Direct Path
NLOS	Non Line-of-Sight
PM	Phase Modulation
QPSK	Quadrature Phase Shift Keying
ROC-MUSIC	Robust Covariation - Based MUSIC
RSS	Received Signal Strength
SNR	Signal-to-Noise Ratio
SOS	Second Order Statistics
TOA	Time-of-Arrival
TDOA	Time Difference-of-Arrival
UDP	Undetected Direct Path
WLAN	Wireless Local Area Network
WWAN	Wireless Wide Area Networks
ZMNL	Zero-Memory Non-Linearity

1. INTRODUCTION

1.1. Background and Motivation

The incredible success of the cellular communications systems and the recent advances in micro and nano technology have increased the demand for positioning services. The location estimation of objects has been studied for over decades in radar and sonar applications. The recent technological advances in electronics and wireless communications and the increasing popularity of wireless networks have almost made the location-based services mandatory. For instance, FCC requires that the wireless communications operators must provide the position of users who emit E911 emergency calls with an accuracy of few tens of meters.

In a localization scenario, generally there are a few base stations who know their positions, and an object-to-be-located. It measures its distance to each base station via several information such as TOA (Time of Arrival), TDOA (Time Difference of Arrival), AOA (Angle of Arrival), or RSSI (Received Signal Strength Indicator). As a result, by combining those distance information, the position of the object is estimated via trilateration or triangulation. Such location estimators are called distance or range-based.

Positioning systems can be classified in many ways. A classification can be proposed as follows:

1. Localization based on Cellular Networks
2. Localization based on GPS (Global Positioning System)
3. Localization based on Wireless Sensor Networks
4. Localization based on Hybrid Systems

GSM (Global System for Mobile communication), the most common 2G (2nd Generation) cellular communications standard in Europe, uses TDOA measurements in order to locate its subscribers. In TDOA, the time difference between signals travelling from two different BTSs (Base Transceiver Stations) to an MS (Mobile Subscriber) is measured. E-OTD (Enhanced Observed Time Difference of Arrival), name of the GSM positioning service based on TDOA, is becoming a de facto standard for E911 Phase II implementation for GSM carriers. The accuracy of the GSM localization service is affected by several factors such as the relative positions of a BTS and an MS, and the multipath radio channel.

GPS, a well-known positioning service, is based on MEO (Medium Earth Orbit) satellites. An object carrying GPS receiver communicates with at least four GPS satellites and measures TOAs of signals coming from them. As a result, by trilateration, it determines its 3D position. Although GPS provides quite accurate location estimates, it requires LOS (Line-of-Sight) communication between the GPS subscriber and the satellites, therefore, it does not work in indoor environments.

The recent advances in MEMS (Micro-Electro-Mechanical-Systems)and wireless communications have created large wireless sensor networks consisting of low-power, low-cost, tiny sensor nodes that have communicating, sensing, and computing capabilities. The sensor nodes can be randomly deployed over the area of interest, and cooperate to fulfill their task. The sensor networks can be used both in commercial and military applications. Environmental monitoring, health, surveillance, and target tracking are application areas for sensor networks. Node localization is one of the most challenging problems for wireless sensor network designers. Although there are many solution proposals in the literature, the problem has not been overcome yet due to the design factors of sensor nodes such as low cost, low power, and small size. The location algorithms for wireless sensor networks can broadly be categorized as beacon-based and beacon-free. In the first group, the network consist of a few beacon nodes that know their positions a priori, and nodes with unknown positions that can be named as blindfolded devices [10]. The beacon nodes may have GPS receivers. Those blindfolded devices estimate the range between themselves and the beacon nodes via TOA, RSSI, or AOA, and calculate their positions. At least three beacon nodes must be in the communicating range of a blindfolded device in order to estimate its position. Once a node determines its position, it becomes a beacon node itself. Due to the nature of the wireless sensor networks, the number of beacon nodes in a network must be as low as possible. For this purpose, mobile beacons can be used. On the other hand, there may be an application scenario where GPS is unavailable and nodes are randomly dispersed over the area. In such a case, a beacon-free localization method is required. Here, a random initial coordinate is assigned to each node in the network. Then, they cooperate with each other and make local distance estimations to learn a coordinate assignment. The ultimate coordinate assignment has both translation and orientation degrees of freedom has to be accurately scaled. Also, there is a need for converting the translation and orientation coordinate assignment to absolute position information.

Today, hybrid positioning systems that combine two or more of those three localization systems have emerged for more accurate and cheaper systems. The combination of sensor networks, GPS, and cellular networks gives better positioning services.

Particularly for distance-based location estimation technologies, the most crucial part of the positioning mechanism is to accurately model the operational environment. The relative positions of the transmitter and receiver, the objects in the environment, mobility of the objects, and the environmental noise have significant effects on the performance of the estimator. In this thesis, the effect of the noise in the environment will be analyzed. In many signal processing applications, environmental noise has been assumed to have Gauss distribution due to the analytical advantages of Gauss assumption. On the other hand, recent studies have shown that underwater acoustic signals, and many types of artificial noise signals all have non-Gauss distribution [3]. In [13], [8], and [14], the receivers designed under the Gauss assumption have shown to fail when they face non-Gaussian noise, which has impulsive nature. This thesis focuses on the impact of the non-Gaussian noise on TOA estimation for indoor positioning purposes.

1.2. Literature Review

There is considerable research on location finding both for indoor and outdoor environments. Particularly, recent developments in wireless communications have increased the popularity of location-based services. GPS is today's most popular positioning technology based on MEO class satellites. However, it does not give accurate location information in indoor environments. The difference between outdoor and indoor radio communication channel characteristics make it impossible to easily adopt a geo-location application designed for outdoor to indoor, and vice versa.

Positioning may be critical for many indoor applications [9]. For instance, it may be used to track children or disabled people in a residence. Also, it may be useful in hospitals where location information of patients is important. Furthermore, it may be needed for tracking fire-fighters or policeman inside a building. Also, it can be used during the security operations against terrorists' attacks on specific buildings.

Especially for range-based positioning services, the multipath nature of indoor radio channel and environmental noise severely affect the performance of the positioning algorithms. In literature, many efforts have focused on modelling the indoor multipath radio channel and estimating TOA. The most widely used channel modelling technique is to collect measurements and then to define a statistical model from measurements. In [17], the measurements of the frequency response of the indoor radio channel in 1 GHz band are done with a network analyser and the relative path loss envelope and phase of a 945 MHz CW (Continuous Wave) signal are described. The channel is modelled by taking the inverse FFT of the frequency response of the measured data. Before IFFT, windowing is used.

In [4], two super-resolution methods, namely, Minimum-norm and autoregressive (AR), and FIR (Finite Impulse Response) filter design on frequency-domain data are employed to estimate the impulse response of the channel. It is shown that AR and minimum-norm models estimate the peak locations and amplitudes of the channel-impulse response while the FIR estimator gives a sampled impulse response estimate whose roots are null locations of the channel frequency response. It is claimed that FIR filter frequency response matching method outperforms both the AR and minimum-norm methods. All three techniques give better time-domain resolutions than the Fourier estimator and typical time-domain measurement systems.

In [5], two blind techniques for simultaneous estimation of the direction-of-arrival (DOA) and the channel parameters for a uniform linear array in a multipath environment are presented. While the first method is based on the sum of weighted complex exponentials and Padé approximation, the second defines the transfer function of a linear time-invariant system given its impulse response. Cramér-Rao lower bound (CRLB) is also derived for the estimator. The environmental noise is assumed to be signal-dependent and Gaussian distributed.

The super-resolution TOA estimation on frequency-domain data with diversity technique is studied in [16] for indoor geo-location applications. MUSIC (MUltiple Signal ClassifICation) is used as a high-resolution method and its performance is compared to the performance of traditional TOA estimation techniques which are IFFT (Inverse Fast Fourier Transform) and cross-correlation technique with DSSS (Direct Sequence Spread Spectrum) signals (DSSS/xcorr). It applies MUSIC to the measured channel frequency response to accurately estimate TOA. It also evaluates the effect of diversity techniques on the performance of super-resolution techniques. It shows that high-resolution techniques significantly improve the performance of TOA estimation as compared to IFFT and DSSS/xcorr. It is also shown that signal bandwidth affects the performance of TOA estimation. According to simulation results, as bandwidth increases, the all three techniques mentioned in the paper show similar performances.

One significant parameter of the receiver design in wireless communications is the model of the additive noise. In both [16] and [4], it is assumed that noise has Gaussian distribution. Their methods are based on the finite second-order statistics of the data. Also other problems such as high-resolution direction finding, detection of the number of sources illuminating an array of sensors, the frequency estimation of several sinusoids have been studied on the Gaussian model basis [3]. Gaussian assumption gives analytically closed-form solutions almost in each situation. However, recent signal modelling studies have showed that many undesired signals in the environment have an impulsive nature [3].

Considering real-world applications, in some environments, especially indoor, noise may not fit the Gaussian model. As a result, a receiver designed on the basis of second-order statistics may fail. Developing signal processing methods for a larger class of random processes which include the Gaussian as a special case will make it possible to maintain good operation of the system in non-Gaussian environments.

Recently, in a significant number of signal processing studies, the class of stable distributions have been used in order to model signals with impulsive nature. Those distributions include Gaussian signals as a special case and are described by their *characteristic exponent* α where $0 < \alpha \leq 2$. When $\alpha = 2$, it becomes Gaussian distribution. Stable distributions have heavier tails than the Gaussian distribution and they do not have finite pth order moments for $p \geq \alpha$. Therefore, second order statistics cannot be used for parameter estimation under impulsive noise. Especially man-made and artificial noise signals in the environment possibly have impulsive nature, and therefore they are modelled well by the stable distribution family.

In [13], MUSIC is used for bearing estimation in the presence of impulsive noise modeled as a complex *symmetric alpha-stable* ($S\alpha S$) process. It also assumes that the signal is complex $S\alpha S$ with the same *characteristic exponent* α as noise. The so-called *covariation matrix* based on the fractional-lower order moment (FLOM) is defined and eigendecomposition-based MUSIC algorithm is applied to the sample covariation matrix to obtain the bearing information from the measurement data. The proposed method, named as ROC-MUSIC (Robust Covariation-Based MUSIC), is compared with traditional SOS-MUSIC (Second-Order-Statistics-based MUSIC), and it is shown that the former significantly outperforms the latter.

Fractional-lower order moment (FLOM)-based matrices that can be used with MUSIC are proposed in [14] to estimate the direction-of-arrivals (DOA) of independent circular signals under additive $S\alpha S$ noise. The main difference between [13] and [14] is that the latter does not model the signal as $S\alpha S$. It claims that communication signals do not possess stable distributions, because they have finite variance. It presents three scenarios that contain circular signals (phase modulation (PM), circularly symmetrical Gaussian, and quaternary phase-shift keying (QPSK)) and one scenario that contains non-circular signals (binary phase-shift keying (BPSK)) all contaminated by the same $S\alpha S$ noise. Simulation results show that the last scenario has poor performance, indicating that FLOM-MUSIC is limited to circular signals. It also compares the performance of proposed FLOM-MUSIC with ROC-MUSIC and reveals that they have similar performances.

In [8], subspace-based frequency estimation of sinusoidal signals contaminated by impulsive noise is presented. It models the noise as an α-stable process and uses the fractional lower order statistics (FLOS) of the data to estimate the signal parameters. It makes two proposals: The first is a FLOS-based statistical average, the generalized covariation coefficient (GCC). It is shown that the GCCs of multiple sinusoids for unity moment order in $S\alpha S$ noise attain the same form as the covariance expressions of multiple sinusoids in white Gaussian noise. FLOS-MUSIC and FLOS-Bartlett are applied to the GCC matrix of the data. Moreover, it is shown that the multiple sinusoids in $S\alpha S$ can also be modeled as a stable autoregressive moving average process approximated by a higher order stable autoregressive (AR) process. The simulation results show that techniques based on lower order statistics are superior to their second-order statistics-based counterparts, especially when the noise shows a strong impulsive attitude.

1.3. Thesis Outline

The rest of the thesis is organized as follows. In Chapter 2, the α-stable random processes are introduced and their mathematical properties are given. Chapter 3 gives information about radio communications and multipath channels. Also, the effect of the multipath communications is introduced. Chapter 4 presents the proposed solution for the TOA estimation for geo-location under impulsive noise. The step-by-step derivation is given. In chapter 5, the validation of the proposed solution based on the simulation results is presented. The performance of the estimator is evaluated based on several parameters, and it is shown that it outperforms the SOS-MUSIC TOA estimator under impulsive noise. Finally, Chapter 6 gives the concluding remarks and the road-map of the future work.

2. ALPHA-STABLE DISTRIBUTIONS

2.1. Introduction

So far, non-Gaussian assumption in signal processing have attracted little attention and Gaussian distribution has been accepted as the basic signal model in most areas of engineering and science due to the fact that it has nice analytical properties, and gives closed-form solutions.

Non-Gaussian distributions have computational complexity and they do not have closed-form solutions. On the other hand, recent technological developments both in software and hardware have made it feasible to model some signals as non-Gaussian where Gauss assumption does not fit the environmental noise. Especially, in some specific applications where Gaussian assumption leads to inaccuracy, it is necessary to adopt non-Gauss assumption.

In signal processing applications, the target is to extract the desired information from observed data contaminated by environmental noise. Due to the fact that the noise has a random nature, stochastic methods play an important role in the signal processing. The appropriate noise model increases the accuracy of the design.

In most wireless communications applications, environmental noise is modelled as additive white Gaussian process for not only it significantly simplifies the design and performance analysis of the receiver but also the Central Limit Theorem mostly justifies the assumption. On the other hand, most of signals and noise sources of real-world applications are definitely non-Gaussian [3]. Underwater acoustic signals, low-frequency atmospheric noise, and many types of man-made noise are found to be non-Gaussian [3]. The severe performance degradation is inevitable for systems designed under Gaussian assumption where the signals in real-case are non-Gaussian. As an example, consider the matched filter for coherent reception of a deterministic signal in additive white Gaussian noise (AWGN). Deviation of noise statistics from Gaussian model leads to the inaccuracy, such as increased false alarm rate or error probability [3]. On the other hand, a receiver designed by nonlinear signal processing based on the actual noise statistics may lead to a more accurate receiver than the matched filter. As a result, there is a trade-off between the accuracy and the computational complexity.

2.2. Signal Processing Applications Based on α-Stable Distributions

Although the stable distribution concept was first introduced by Levy in the study of generalized central limit theorem in 1925, it was not considered for signal processing applications until the middle of 1970s. The main reason of ignoring stable distributions in signal processing is the fact that they do not have closed-form pdf expressions except for $\alpha = 1$ and $\alpha = 2$ which are Cauchy and Gaussian distributions, respectively. For the rest of the stable random variables, power series expansions are used to obtain their probability density functions. Another reason is that the second and higher order statistics do not exist for α-stable random variables. Most signal processing applications rely on the second and higher order statistics of data.

Although the Gaussian assumption was dominant against α-stable distributions, in recent years, stable distributions have applied to significant number of applications in physics, economics, biology and electrical engineering.

In 1919, the Danish Astronomer Holtsmark discovered that random fluctuations of gravitational fields of stars in space under certain natural assumptions obey the stable law with $\alpha = 1.5$. It was one of the first applications of stable distributions. In the middle of 1960s, the work done by Mandelbrot in economics and finance opened a new era for the application of stable distributions. He proposed a revolutionary approach based on stable distributions to the problem of price movement where Gasussian assumption and least-square criterion failed. Many financial variables, such as common stock price changes, fluctuations in speculative prices, and interest rates have been shown to closely obey to non-Gaussian stable laws [3]. The stable distribution has also applied to the signal processing and communications applications. Mandelbrot and Van Ness used Gaussian and stable fractional stochastic processes to describe longrange dependence arising in engineering, economics, and hydrology. What is more, it has been used to obtain the patterns of error clustering in telephone circuits [3].

It is accepted that the traditional additive Gaussian noise assumption is inadequate because of the occurrence of noise with low probability but large amplitudes. Therefore, the stable distribution that fits better this reality should get more attention.

2.3. α-Stable Distribution Family and Density Functions

Most real-world non-Gaussian signals have impulsive nature where those kind of signals produce large-amplitude excursions from the average value more frequently than Gaussian signals. Their probability density functions (pdf) have heavier tails than the Gaussian pdf. Stable distributions provide a useful mean for this type of signals. The stable law is a generalization of the Gaussian distribution and includes it as a limiting case. The heavier tails of the stable density unveils the difference between them.

A stable distribution is mainly determined by the *characteristic exponent* α $(0 < \alpha \leq 2)$. As α decreases, impulsiveness of the signal increases. $\alpha = 2$ and $\alpha = 1$ represent the Gaussian and Cauchy distributions, respectively. Figure 2.1 shows the probability density function of an α-stable random variable for different values of α [3].

It is well known that statistical moments of signals are useful tools for obtaining the desired information in signal processing applications. The conventional spectral estimation methods based on Gaussian assumption exploit the second order statistics of the observed data in order to extract needed information. Also, higher order statistics, such as third and fourth order, based signal processing techniques are very useful. However, stable distributions do not possess finite moments of the order higher than two. It means that the variance does not exist for signals with $\alpha < 2$. As a result, many methods for signal processing applications based on second order statistics are invalid for stable distributions. Therefore, they require so called *fractional lower order moments (FLOM)* that have a moment order p $p < \alpha$. Instead of variance, the *dispersion* of an *α-stable* random variable plays an important role. The larger *dispersion*

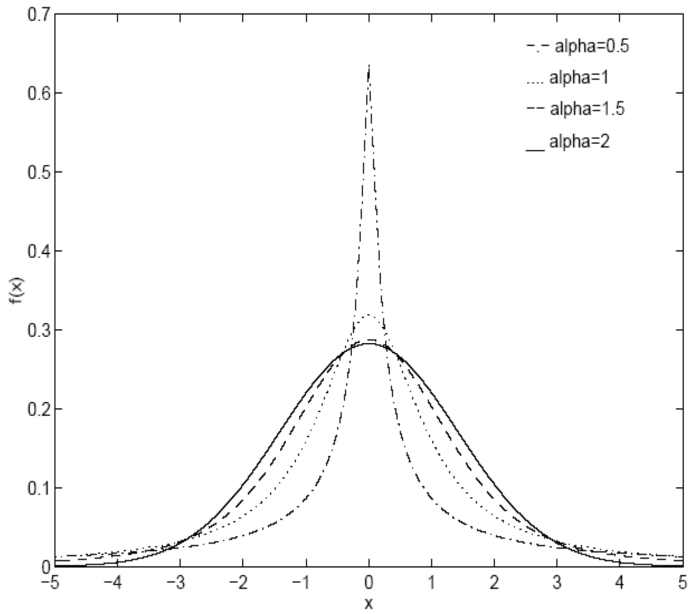

Figure 2.1. Density functions of an α-stable random variable for different α's

implies more spread around the median of the distribution. Hence, the minimum *dispersion* criteria is desired. Minimum *dispersion* means minimum fractional lower-order moments of estimation errors which is the measure of the distance between the true value and its estimate.

As observed from Figure 2.1, $S\alpha S$ densities have similar features with the Gaussian densities, such as being smooth, unimodal, symmetric with respect to the median, and bell-shaped. On the other hand, for small absolute values of x, the $S\alpha S$ densities are sharper than the densities of normal distributions. In other words, the stable densities have algebraic tails while Gauss density has exponential tails [3]. The heavier tails of the stable densities justifies the idea of using them to model non-Gaussian signals in real world because in many signal processing applications, although non-Gaussian signals are similar to the Gauss, they have heavier tails [3].

The best way of describing the stable distribution is to determine its *characteristic function*, because it does not have a closed-form solution of the probability distribution function.

The characteristic function of a univariate α-stable distribution function, denoted by *F(x)*, is given by

$$\varphi(t) = \exp\{jat - \gamma|t|^{\alpha}[1 + j\beta \mathrm{sign(t)}\omega(\mathrm{t},\alpha)]\} \tag{2.1}$$

Here

$$\omega(t,\alpha) = \begin{cases} \tan\frac{\alpha\pi}{2} & \text{if} \quad \alpha \neq 1, \\ \frac{2}{\pi}\log|t| & \text{if} \quad \alpha = 1. \end{cases} \tag{2.2}$$

$$\mathrm{sign(t)} = \begin{cases} 1 & \text{if} \quad \mathrm{t} > 0 \\ 0 & \text{if} \quad \mathrm{t} = 0 \\ -1 & \text{if} \quad \mathrm{t} < 0 \end{cases} \tag{2.3}$$

and

$$-\infty < a < \infty, \qquad \gamma > 0, \qquad 0 < \alpha \leq 2, \qquad -1 \leq \beta \leq 1 \tag{2.4}$$

As seen from (2.12), for a complete determination of a stable characteristic function, four parameters, $(\alpha, a, \beta, \gamma)$, are needed. They are defined as follows:

1. α is the characteristic exponent and is uniquely determined. It has a value between (0,2] and defines the thickness of the tails of the distribution. If $\alpha = 2$, the distribution is Gaussian and if $\alpha = 1$, the distribution is Cauchy.
2. γ is the dispersion, also named as scale parameter ($\gamma > 0$). It is similar to the variance of the Gaussian distribution. For Gaussian case, it is half the variance of that Gauss random variable.
3. β is the symmetry parameter. If $\beta = 0$, the distribution is called *symmetric*

α-*stable*, ($S\alpha S$). The Gaussian and the Cauchy distributions are both $S\alpha S$.

4. a is the location parameter. For $S\alpha S$ distributions, it is the mean when $1 < \alpha \leq 2$, and the median when $0 < \alpha < 1$.

A stable distribution is called *standard* if $a = 0$ and $\gamma = 1$. Figure 2.2 shows different $S\alpha S$ time series depending on α. It is apparent that as α increases, the signal gets more impulsive and has higher amplitude values.

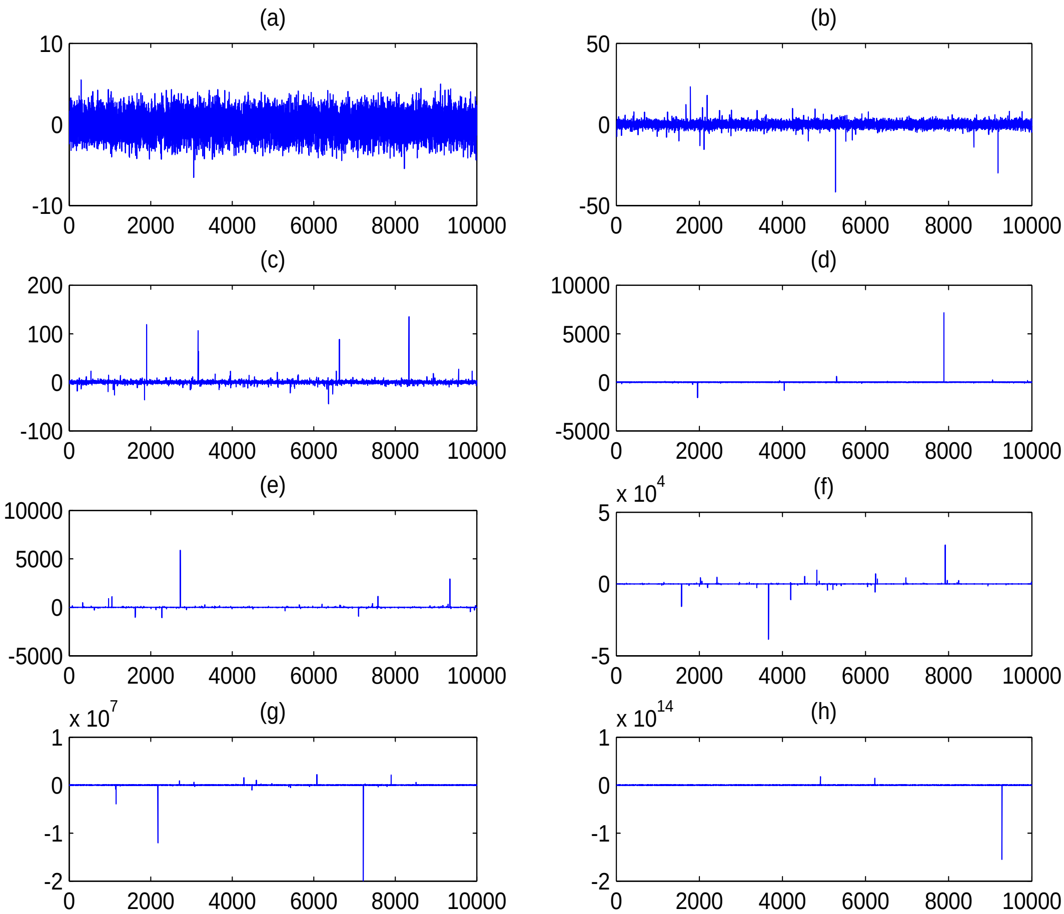

Figure 2.2. Different $S\alpha S$ Time Series for a: $\alpha = 2$ (Gauss),b: $\alpha = 1.9$, c: $\alpha = 1.7$, d: $\alpha = 1.3$, e: $\alpha = 1.0$ (Cauchy), f: $\alpha = 0.8$, g: $\alpha = 0.5$, h: $\alpha = 0.3$

The probability density function of a standard stable random variable is readily obtained by taking the inverse Fourier transform of its characteristic function.

$$f(x; \alpha, \beta) = \frac{1}{\pi} \int_0^{\infty} \exp(-t^{\alpha}) \cos[xt + \beta t^{\alpha} \omega(t, \alpha)] dt \tag{2.5}$$

Due to the fact that Fourier transform has the symmetry property, $f(x;\alpha,\beta) = f(-x;\alpha,-\beta)$. Zolotarev studies the derivatives of the (2.5) and shows that they are bounded [3].

The stability property and the generalized central limit theorem are the two important properties of the stable distributions. They are defined as follows:

1. Stability Property: A random variable X is stable if and only if for any independent random variables X_1, X_2 with the same distribution as X, and for arbitrary constants a_1, a_2, there exist constants a and b such that

$$a_1X_1 + a_2X_2 \underline{\underline{d}} \; aX + b \tag{2.6}$$

where '$\underline{\underline{d}}$' implies that the terms at two sides have the same distribution.

2. Generalized Central Limit Theorem: X is the limit in distribution of normalized sums of the form

$$S_n = (X_1 + \ldots + X_n)/a_n - b_n \tag{2.7}$$

where X_1, X_2, ... , are i.i.d. and $a_n \to \infty$, if and only if X is stable.

As mentioned before, there is no closed-form expression for the general stable density and distribution functions, except for the Gaussian ($\alpha = 2$), Cauchy ($\alpha = 1, \beta = 0$), and Pearson ($\alpha = 1/2, \beta = -1$) distributions [3]. For the rest of the stable distributions, the approximate stable density functions are obtained by using power series expansions. For $x > 0$, the standard stable density function is given by

$$f(x;\alpha,\beta) = \begin{cases} \frac{1}{\pi x}\sum_{k=1}^{\infty}\frac{(-1)^{k-1}}{k!}\Gamma(\alpha k+1)(\frac{x}{r})^{-\alpha k}\sin[\frac{k\pi}{2}(\alpha+\zeta)], & 0<\alpha<1 \\ \frac{1}{\pi x}\sum_{k=0}^{\infty}\frac{(-1)^{k-1}}{k!}\Gamma(\frac{k}{\alpha}+1)(\frac{x}{r})^{k}\sin[\frac{k\pi}{2\alpha}(\alpha+\zeta)], & 1<\alpha\leq 2 \end{cases} \tag{2.8}$$

where

$$\eta = \beta \tan(\pi\alpha/2), r = (1+\eta^2)^{-1/(2\alpha)}/, \zeta = -(2/\pi)\arctan\eta. \tag{2.9}$$

and $\Gamma(\cdot)$ is the gamma function defined by

$$\Gamma(x) = \int_0^\infty t^{x-1}e^{-t}dt. \tag{2.10}$$

For the standard symmetric α-stable *(SαS)* distributions, the density function reduces to

$$f_\alpha(x) = \begin{cases} \frac{1}{\pi x}\sum_{k=1}^{\infty}\frac{(-1)^{k-1}}{k!}\Gamma(\alpha k+1)|x|^{-\alpha k}\sin[\frac{k\pi\alpha}{2}], & 0<\alpha<1 \\ \frac{1}{\pi\alpha}\sum_{k=0}^{\infty}\frac{(-1)^k}{2k!}\Gamma(\frac{2k+1}{\alpha})x^{2k}, & 1<\alpha\leq 2. \end{cases} \tag{2.11}$$

The behavior of $S\alpha S$ and Gaussian densities are similar near the origin, however, the tails of the first decays at a lower rate than the latter. The densities of an impulsive signal have algebraic tails, whereas the Gaussian density has exponential tails. As the characteristic exponent α decreases, the tail of the $S\alpha S$ density becomes heavier, that is, highly impulsive signals have small characteristic exponent α. This is the reason for why $S\alpha S$ densities are suitable for modelling impulsive noise and signals.

The symmetric α-stable ($S\alpha S$) distribution is defined by its characteristic function

$$\varphi(\omega) = \exp(j\delta\omega - \gamma|\omega|^\alpha) \tag{2.12}$$

The pdf of Gaussian and Cauchy distributions for a random variable x are given below respectively,

$$f_1(\gamma,\delta;x) = \frac{1}{\pi}\frac{\gamma}{\gamma^2+(x-\delta)^2} \tag{2.13}$$

$$f_2(\gamma, \delta; x) = \frac{1}{\sqrt{4\pi\gamma}} \exp[-\frac{(x-\delta)^2}{4\gamma} \tag{2.14}$$

2.4. Bivariate Isotropic Stable Distributions

The definition of the multivariate stable distributions are done via the stability property. Let $F(x)$ be a k-dimensional distribution function where $x \in \mathbb{R}$. It is stable if, for any i.i.d random vectors $\mathbf{X}_1$, $\mathbf{X}_2$ with distribution function F_x and arbitrary constants a_1, a_2, there exist $a \in \mathbb{R}$, $\mathbf{b} \in \mathbb{R}$ and a random vector $\mathbf{X}$ with the same distribution function $F(x)$ such that

$$a_1\mathbf{X}_1 + a_2\mathbf{X}_2 \underline{\underline{d}} a\mathbf{X} + \mathbf{b}. \tag{2.15}$$

While the family of one-dimensional stable distributions forms a parametric set, the family of multivariate stable distributions forms a nonparametric set [3].

Multidimensional isotropic stable distribution is an exception which can be readily defined. Bivariate isotropic stable distributions have been used as the model of the noise in signal processing applications with impulsive noise [13], [14].

The characteristic function of a bivariate isotropic α-stable distribution is given by

$$\varphi(\omega_1, \omega_2) = \exp(j(\delta_1\omega_1 + \delta_2\omega_2) - \gamma|\omega|^\alpha) \tag{2.16}$$

where $\omega = (\omega_1, \omega_2)$ and $|\omega| = \sqrt{\omega_1^2\omega_2^2}$.

Note that α and γ are the characteristic exponent and the dispersion, respectively. δ_1 and δ_2 are the location parameters. The distribution is isotropic with respect to the point (δ_1,δ_2). The two marginal distributions of the isotropic stable distribution are SαS with parameters $(\delta_1, \gamma, \alpha)$ and $(\delta_2, \gamma, \alpha)$.

2.5. Fractional-Lower Order Moments (FLOMs) and Covariations of Symmetric α-Stable Processes

It is known that only moments of order less than α exist for the non-Gaussian $S\alpha S$ distribution family. Let p denote the moment order and assume that the α-stable distributions are symmetric ($\beta = 0$) and centered around the origin ($a = 0$). In many signal processing applications, second-order statistics (SOS) play an important role, however, they do not work for non-Gaussian signals due to their infinite variance. In this section, the fractional-lower order moments (FLOMs) and covariations which will be used in signal processing applications with non-Gaussian signals are introduced. Before going into details, it is worthy to give some basic types of the stable processes, because there are many types of them. Two most popular of them are as follows:

1. Sub-Gaussian Processes: A stable process $X(t),\ t \in T$ is an α-sub-Gaussian process (α-SG(R)), if for all $n \geq 1$ and different indices $t_1, ..., t_n$, $(X(t_1), ..., X(t_n))$ has the following characteristic function

$$\varphi(\mathbf{u}) = \exp(-[\frac{1}{2}\sum_{l,m=1}^{n} u_l u_m R(t_l, t_m)]^{\alpha/2}) \tag{2.17}$$

Here $R(t, s)$ is a positive-definite function, $\mathbf{u} = [u_1, ..., u_n]^T$, and $\alpha\epsilon(1, 2]$. If $R(t, s) = R(t - s) = R(s - t)$, the sub-Gaussian process is stationary. Actually, sub-Gaussian processes are variance mixtures of Gaussian processes [3]. When $X(t)$ is α-SG(R), then $X(t)$ is re-written as follows

$$X(t) = S^{1/2}Y(t) \tag{2.18}$$

where S is a positive stable random variable with characteristic exponent equal to $\alpha/2$, and $Y(t)$ is a Gaussian process with zero-mean and covariance function $R(t, s)$.

2. Linear Stable Processes: Let $U(n), n = 0, \pm1, \pm2, \ldots$ be a family of i.i.d $S\alpha S$ random variables. $X(n) = \sum_{i=-\infty}^{\infty} a_i U(n - i)$ is a stationary $S\alpha S$ random process

if $\sum_{i=-\infty}^{\infty} |a_i|^{\alpha-\delta} < 0$ for some $0 < \delta < \alpha$ when $0 < \alpha < 1$, or if $\sum_{-\infty}^{\infty} |a_i| < \infty$ when $\alpha \geq 1$. Finite-order autoregressive (AR), moving-average (MA), and autoregressive moving-average (ARMA) processes are the examples of linear stable processes.

2.5.1. Fractional Lower Order Moments (FLOMs) of Symmetric α-Stable Processes

The fractional lower order moment (FLOM) for $S\alpha S$ random variable with zero location parameter and dispersion γ is defined as follows:

Let X be a $S\alpha S$ random variable with zero location parameter and dispersion γ. Then the FLOM is given by

$$E|X|^p = C(p,\alpha)\gamma^{\frac{p}{\alpha}} \tag{2.19}$$

for $0 < p < \alpha$ where

$$C(p,\alpha) = \frac{2^{p+1}\Gamma(\frac{p+1}{2})\Gamma(-\frac{p}{\alpha})}{\alpha\sqrt{\pi}\Gamma(-\frac{p}{2})} \tag{2.20}$$

and $\Gamma(\cdot)$ is the Gamma function defined in (2.10).

The interesting point of (2.19) is that it is independent of X. For the proof of (2.19) and (2.20), please see [3].

2.5.2. Covariations of Symmetric α-Stable Processes

The second-order statistics of data play a prominent role in the signal processing applications. Filtering, signal detection and estimation and many other statistical signal processing applications rely on the correlation and covariance concepts. As stated before, α-stable distributed signals do not have finite variance, that is, covariance is nonsense. Instead, so-called *covariation* has been proposed by Miller and Cambanis [3].

Note that *covariation* plays a similar role for $S\alpha S$ as covariance plays for Gaussian random variables.

Assume that X and Y are jointly $S\alpha S$ with $1 < \alpha \leq 2$. The *covariation* of X with Y is given by

$$[X,Y]_\alpha = \int_S xy^{<\alpha-1>}\mu(d\mathbf{s}) \tag{2.21}$$

where S is the unit circle and $\mu(\cdot)$ is the spectral measure of the $S\alpha S$ random vector *(X, Y)*. For any real number z and $a \geq 0$, the following notation is used

$$z^{<a>} = |z|^a \mathrm{sign(z)} \tag{2.22}$$

In particular, $z^{<0>} = \mathrm{sign(z)}$.

On the other hand, the covariation coefficient of X with Y is defined by

$$\lambda_{X,Y} = \frac{[X,Y]_\alpha}{[Y,Y]_\alpha} \tag{2.23}$$

Let X and Y be jointly $S\alpha S$ with $1 < \alpha \leq 2$. Assuming that the dispersion of Y is γ_y [3],

$$[Y,Y]_\alpha = \|Y\|_\alpha^\alpha = \gamma_y \tag{2.24}$$

$$\lambda_{XY} = \frac{E(XY^{<p-1>})}{E(|Y|^p)} \qquad 1 \leq p < \alpha \tag{2.25}$$

$$[X,Y]_\alpha = \frac{E(XY^{<p-1>})}{E(|Y|^p)}\gamma_y \qquad 1 \leq p < \alpha \tag{2.26}$$

Some significant properties of covariations are given in the following [3].

1. If X_1, X_2 and Y are jointly $S\alpha S$, then the covariation $[X,Y]_\alpha$ is linear and given by

$$[aX_1 + bX_2, Y]_\alpha = a[X_1, Y]_\alpha + b[X_2, Y]_\alpha \tag{2.27}$$

for any real constants a and b.

2. If $\alpha = 2$, the covariation of jointly $S\alpha S$ random variables X and Y reduces to the covariance of jointly Gaussian two random variables X and Y

$$[X,Y]_\alpha = E(XY) \tag{2.28}$$

3. Generally, $[X,Y]_\alpha$ is not linear with respect to the second variable Y. However, the following pseudo-linearity property with respect to Y can be given. If Y_1 and Y_2 are independent and X, Y_1, Y_2 are jointly $S\alpha S$, then

$$[X, aY_1 + bY_2]_\alpha = a^{<\alpha-1>}[X, Y_1]_\alpha + b^{<\alpha-1>}[X, Y_2]_\alpha \tag{2.29}$$

for any real constants a and b.

4. If X and Y are independent and jointly $S\alpha S$, then $[X,Y]_\alpha = 0$ Note that the converse is generally not true.

5. The Cauchy-Schwartz inequality holds for any jointly $S\alpha S$ random variables X and Y and has the following form

$$|[X,Y]_\alpha| \leq \|X\|_\alpha \|Y\|_\alpha^{<\alpha-1>} \tag{2.30}$$

Particularly, if X and Y have unit dispersion, one has $|[X,Y]_\alpha| \leq 1$.

Assume that X and Y are both linear combinations of independent $S\alpha S$ random variables and let U_is be independent $S\alpha S$ random variables with dispersions γ_i, $i = 1, ..., n$. For any numbers $a_1, ..., a_n, b_1, ..., b_n$ where all b_is are not zero

$X = a_1 U_1 + ... + a_n U_n$ and $Y = b_1 U_1 + ... + b_n U_n$

Using the basic properties of covariation

$$[X, X]_\alpha = \gamma_1 |a_1|^\alpha + ... + \gamma_n |a_n|^\alpha \tag{2.31}$$

$$[Y, Y]_\alpha = \gamma_1 |b_1|^\alpha + ... + \gamma_n |b_n|^\alpha \tag{2.32}$$

$$[X, Y]_\alpha = \gamma_1 a_1 b_1^{<\alpha-1>} + \cdots + \gamma_n a_n b_n^{<\alpha-1>} \tag{2.33}$$

$$\lambda_{XY} = \frac{\gamma_1 a_1 b_1^{<\alpha-1>} + \cdots + \gamma_n a_n b_n^{<\alpha-1>}}{\gamma_1 |b_1|^\alpha + \cdots + \gamma_n |b_n|^\alpha} \tag{2.34}$$

2.6. Complex $S\alpha S$ Random Variables and Covariations

In this thesis, the environmental noise is assumed to be complex-valued $S\alpha S$, therefore it is worthy to explain the complex symmetric stable variables.

A complex random variable $\mathbf{X} = \mathbf{X}_1 + j\mathbf{X}_2$ is $S\alpha S$ if $\mathbf{X}_1$ and $\mathbf{X}_2$ are jointly $S\alpha S$. Note that all real and complex $S\alpha S$ have zero-means and $\alpha \epsilon (1, 2]$. The characteristic function of a complex $S\alpha S$ is given by

$$\begin{aligned} \varphi(\omega) = E\{\exp[jRe(\omega X^*]\} = E\{\exp[j(\omega_1 X_1 + \omega_1 X_1)]\} \\ = \exp[-\int_{S_2} |\omega_1 x_1 + \omega_2 x_2|^\alpha d\Gamma_{X_1,X_2}(x_1, x_2)] \end{aligned} \tag{2.35}$$

Let $\mathbf{X} = \mathbf{X}_1 + j\mathbf{X}_2$ and $\mathbf{Y} = \mathbf{Y}_1 + j\mathbf{Y}_2$ be jointly $S\alpha S$. The covariation of X and Y is defined by

$$[X, Y]_\alpha = \int_{S_4} (x_1 + jx_2)(y_1 + jy_2)^{<\alpha-1>} d\mu_{x_1,x_2,y_1,y_2}(x_1, x_2, y_1, y_2) \tag{2.36}$$

where S_4 is the unit sphere in $\mathbb{R}^4$ and $\mu_{x_1,x_2,y_1,y_2}(x_1, x_2, y_1, y_2)$ is the spectral measure of the $S\alpha S$ random vector (X_1, X_2, Y_1, Y_2). For a complex number z and $\beta > 0$, the following convention is used

$$z^{<\beta>} = |z|^{\beta-1} z^* \tag{2.37}$$

where $*$ denotes conjugate. As a result, the covariation coefficient of X with Y is defined by

$$\lambda_{XY} = \frac{[X, Y]_\alpha}{[Y, Y]_\alpha} \tag{2.38}$$

The following properties hold for two complex jointly $S\alpha S$ with zero means and a characteristic exponent α that has a value between $(1, 2]$ [12].

$$E(|X|^p) = \frac{p2^p\Gamma(p/2)\Gamma(-p/\alpha)}{\alpha\Gamma(-p/2)}[X, X]_\alpha^{p/\alpha}, 0 < p < \alpha \tag{2.39}$$

$$\lambda_{XY} = \frac{E(XY^{<p-1>})}{E(|Y|^p)}, 1 < p < \alpha \tag{2.40}$$

$$[X_1 + X_2, Y]_\alpha = [X_1, Y]_\alpha + [X_2, Y]_\alpha \tag{2.41}$$

$$[aX, bY]_\alpha = ab^{<\alpha-1>}[X, Y]_\alpha \tag{2.42}$$

$$[X, Y]_\alpha = 0 \text{ if X and Y are independent.} \tag{2.43}$$

2.7. Generation of Complex Isotropic $S\alpha S$ Random Variables for Simulations

In this thesis, the environmental noise is assumed to be impulsive and it is modelled as the *complex isotropic* $S\alpha S$. Let $X = X_1 + jX_2$ be the complex isotropic $S\alpha S$ random variable of characteristic exponent α ($\alpha < 2$) and dispersion γ. It is generated as follows [12]:

1. Generate a real stable random variable A of characteristic exponent $\alpha/2$, dispersion $\cos^2(\pi\alpha/4)$, and skewness $\beta = 1$. For the generation of a real stable random variable, refer to [12].
2. Generate two i.i.d. zero-mean Gaussian variables G_1 and G_2. They are independent of the real stable random variable A

3. Compute X as follows

$$X = A^{1/2}(G_1 + jG_2) \tag{2.44}$$

Note that the vector (X_1, X_2) is sub-Gaussian with underlying vector $(G_1,\, G_2)$. Also, it can be proven that the real and imaginary parts of X are always dependent, unless G_1 and G_2 are degenerate.

The relationship between the dispersion γ of the complex random variable $X = X_1 + jX_2$ and the variance σ^2 of the complex Gaussian random variable $G = G_1 + jG_2$ is an important point of the generation process of the complex isotropic $S\alpha S$. It is given by

$$\gamma = (\sigma^2/2)^{\alpha}. \tag{2.45}$$

The proof can be found in [12]. In Figure 2.3, 2.4, and 2.5 plots of generated complex isotropic $S\alpha S$ for different characteristic exponent α values are given.

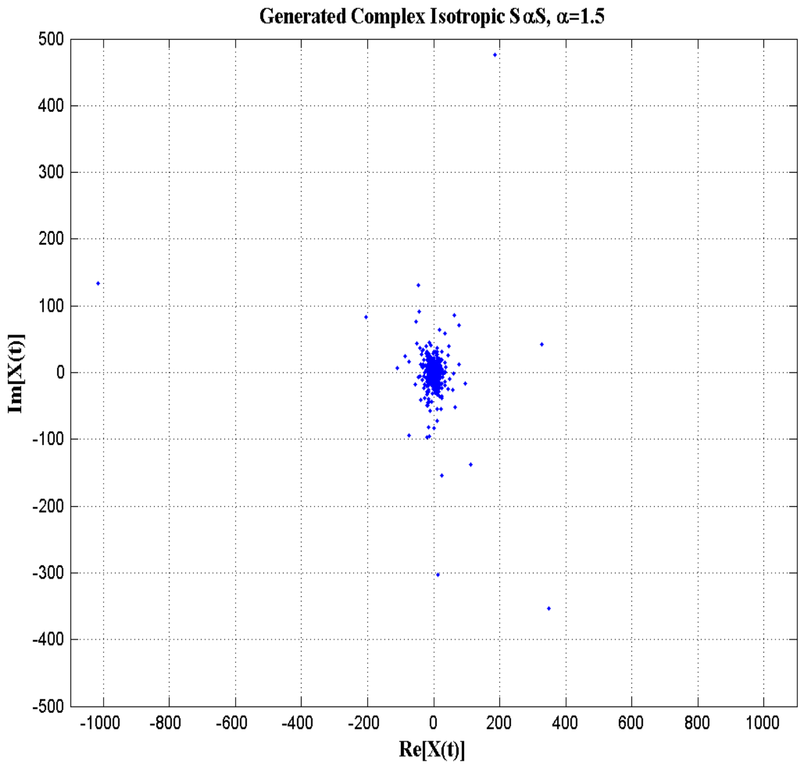

Figure 2.3. Complex Isotropic $S\alpha S$ for $\alpha = 1.5$

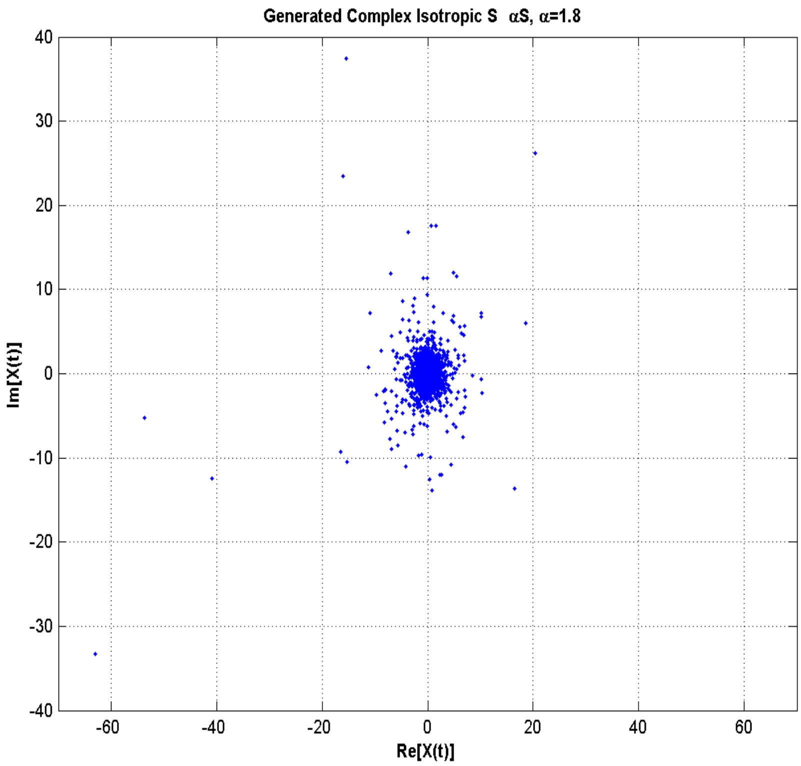

Figure 2.4. Complex Isotropic $S\alpha S$ for $\alpha = 1.8$

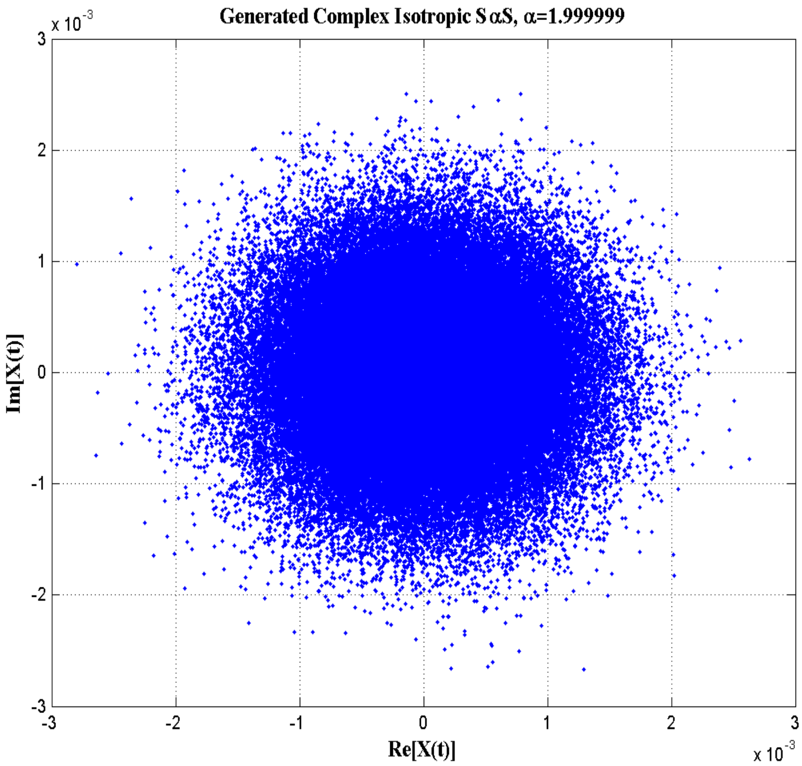

Figure 2.5. Complex Isotropic $S\alpha S$ for $\alpha = 1.999\bar{9}$

3. INDOOR RADIO CHANNEL

Generally, there are two types of communication media namely *guided* and *unguided*. Wired communication is an example of the first group where a reliable link is built between the communicating entities. On the other hand, wireless medium, an example of unguided medium, is unpredictable and has disruptive effects on the communications. It does not provide a reliable communication link. It is impossible to define a unique model to represent all types of wireless communications channels. The importance of the wireless medium stems from the fact that it provides mobile communication, which has become prolific in last decade. Furthermore, it is more flexible compared to wired links. Signals with different frequencies require different wires, however, they can be sent over the same wireless link which is air. Some of the most popular frequencies used by wireless communications technologies are 900 MHz and 1.8 GHz (cellular), 2-5 GHz (WLANs), and 28-60 GHz (microwave).

Roughly speaking, there are two operational environments for wireless communications; indoor and outdoor. In this section, mainly, indoor radio channels will be introduced because the environment where the problem is defined is indoor.

3.1. Radio Communications and Positioning in Indoor Environments

Due to the fact that radio signals with frequencies above 800 MHz have extremely small wavelengths compared with the dimensions of the building features, it is feasible to assume electromagnetic waves as rays [7]. Both indoor and outdoor environments have three main effects on wireless communications: reflection, diffraction and scattering.

The reflection is caused by the ground, walls of buildings, the ceiling and the floor and has the amplitude coefficients usually determined by plane wave analysis. Impinging of electromagnetic waves on obstructions larger than the wavelength causes to the specular reflections. Also the frequency and the angle of incidence, and the nature of the medium contribute to the ray attenuation. Reflections are especially effective in indoor environments. On the other hand, its importance is decreased in outdoor environments due to multiple transmissions that reduce the strength of the signal to negligible values.

Diffracted fields are generated by the edges of buildings, walls and other large objects that act as a secondary wave source and propagate away from the diffracting edge as cylindrical waves. The diffracted component of the signal may reach a receiver, which is not in the line of sight of the transmitter. The strength of a diffracted signal is lowered to much greater levels than the attenuation caused by reflection and transmission. Therefore, diffraction is significant especially for outdoors where signal transmission through buildings is virtually impossible.

Irregular objects such as walls with rough surfaces and furniture of indoors and vehicles, foliage of outdoors cause rays to scatter in all directions in the form of spherical waves. Especially when the dimensions of objects are on the order of a wavelength or less than it, scattering happens. It is not significant when the receiver or sender is not located in a highly cluttered environment. In Figure 3.1 and Figure 3.2, reflection, scattering and diffraction are picturized for indoor and outdoor environments, respectively [7].

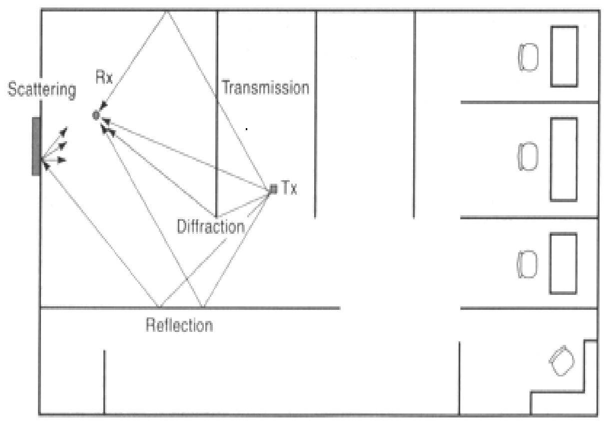

Figure 3.1. Radio Propagation in an indoor environment

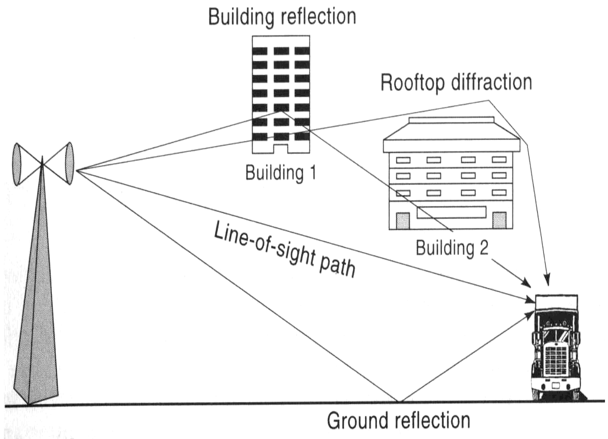

Figure 3.2. Radio propagation in an outdoor environment

3.2. Indoor Radio Channel

The studies for characterizing indoor radio communications have greatly increased due to the recent advances in WWAN and WLAN technologies. Indoor and outdoor communications have different characteristics. First of all, the communication distance in indoor environments is much smaller than that of outdoor. Furthermore, the environmental conditions that determine the radio channel may frequently change. The structure of the building and the positions of the objects in the environment significantly affect the performance of the radio communication system.

Due to scattering, reflection and refraction caused by the structure of environments, multipath fading occurs at receiver. Fading is the rapid fluctuation of the amplitude of a radio signal that happens in a short time interval or distance. Due to fading, different versions of an original signal arriving at receiver at different time instants lead to phase and amplitude distortions on the original signal.

The amplitude and phase of signals arriving at the receiver are random variables. The time-varying behavior of the channel is caused by the motion of the communicating entities or by the movement of the reflectors and scatterers. The movement of objects in the environment, mobile receiver and transmitter have crucial effects on the quality of wireless communication. A mobile receiver with high speed may pass through several fades in a short period of time. As a worst case, receiver can stop at a location at which received signal is in a deep fade where wireless communication may stop.

The relative motion between the receiver and the transmitter causes multipath waves to face frequency change named as Doppler shift. In other words, Doppler shift defines the random frequency modulation caused by the relative motion between receiver and transmitter. It depends on the velocity and direction of those two communicating entities. If receiver moves toward transmitter, Doppler shift will be positive, otherwise it will be negative.

Another parameter creating Doppler shift is the speed of objects in the environment. It introduces a time varying Doppler shift on multipath waves. However, if the velocity of objects is lower than receiver, their effect may be ignored.

The relationship between the bandwidth of the multipath channel and the bandwidth of the transmitted signal has effect on wireless communication. If the latter is larger than the first, the signal is distorted, but fading effect is not significant. For opposite case, signal power will change rapidly but it will not be distorted in time.

The wireless communication designers often choose to model the indoor radio channel statistically instead of trying to eliminate multipath distortions. If the model fits the real case well, the receivers and transmitters designed according to the model can work fine. The success of cellular communications and fast developments in micro and nano technologies increased the demand for wireless communications, that ,as a result, increased the research on the modelling of indoor radio channels. The method is straightforward; once the measurements have collected in the real world, a proper statistical model that fits those measurements are defined. The most widely accepted indoor radio channel model is the impulse response characterization of the multipath fading channel, first suggested by Turin [6].

The multipath fading effect of an indoor radio channel is also called small-scale fading because the amplitude of a radio signal fluctuates over a short period of time or travel distance. The large-scale path loss can be ignored for indoor radio communications [15]. The three significant phenomenon caused by multipath fading are rapid changes in signal strength, random frequency modulation because of varying Doppler shifts on different multipath signal components and echose (time dispersion) caused by multipath propagation delays.

The main factors introducing small-scale fading are speed of surrounding objects, speed of the mobile, the transmission bandwidth of the signal and multipath propagation. The first two factors cause to Doppler shift on signal components while the other two factors cause to signal distortions, rapid changes in signal strength and echoes.

3.2.1. Multipath Indoor Channel Impulse Response

The impulse response completely characterizes the channel and contains all information about it. It was first proposed by Turin for the time-invariant radio channels and found wide acceptance in the literature. It gives the wideband channel characterization of the channel and provides all necessary information for simulating and analyzing any type of radio communication. A linear time-varying filter is used to model the random time-varying indoor multipath channel. Time variation is caused by mobile receiver whereas filtering represents different amplitudes and delays of multipath signals arriving at the receiver at any time instant.

The linear time-varying filter model of the radio channel is given by

$$h(t,\tau) = \sum_{k=0}^{P-1} b_k(t)\delta(\tau - \tau_k(t))e^{j\theta_k(t)} \tag{3.1}$$

where t stresses the time-variation of the channel, P is the number of multipaths, $b_k(t)$, $\tau_k(t)$, and $\theta_k(t)$ are the random time-varying amplitude, arrival-time and phase sequences, respectively. For the complete characterization of the channel, those three parameters are needed. t and τ are the observation time and application time of the impulse, respectively. $\delta(\cdot)$ is the Dirac delta function.

The channel can be characterized by using discrete-time impulse response where the time axis is divided into small time intervals named as "bins" [6]. It is assumed that each bin either has one multipath signal component or not. In other words, due to the fact that $b_k(t,\tau)$ may be zero, some excess delay bins may not have multipath and delay τ_k at some time t . In Figure 3.3, a multipath channel example at different snapshots is given where t varies into the page, and the time delay bins are quantized to widths of $\Delta\tau$. Due to the fact that two paths arriving within a bin cannot be resolved as distinct paths, the bin size should be chosen as the resolution of the specific measurement. In this model, each impulse response is described by a sequence of "0"s and "1"s where a "1" indicates the presence of a path in a given bin and a "0" represents the absence of a path in that bin. Each "1" is associated with an amplitude and a phase value. The simulation of any indoor wireless communication system can be done with this model. The objects in the environment are possibly in motion in a real situation; however the

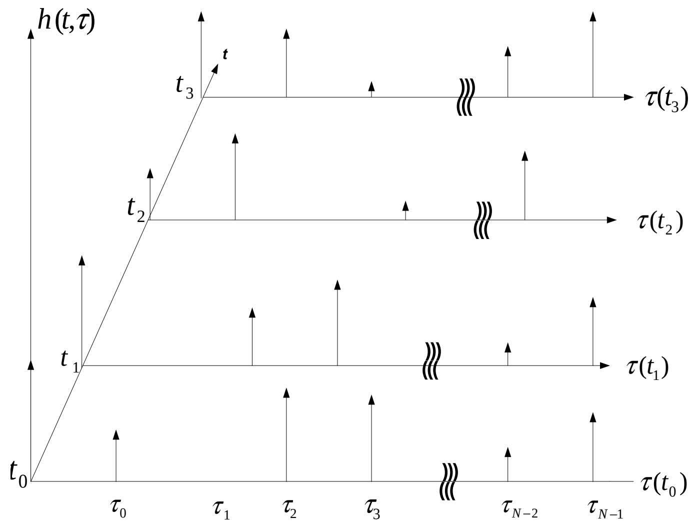

Figure 3.3. Time-varying discrete-time impulse response of a multipath radio channel

channel variation is relatively slow compared to the signal rate, therefore, the channel parameters can be assumed as time-invariant random variables [16]. The mathematical representation of the time-invariant radio channel is given by

$$h(t) = \sum_{k=0}^{P-1} b_k e^{j\theta_k} \delta(t - \tau_k) \tag{3.2}$$

which is the complex, low-pass channel impulse response of the channel.

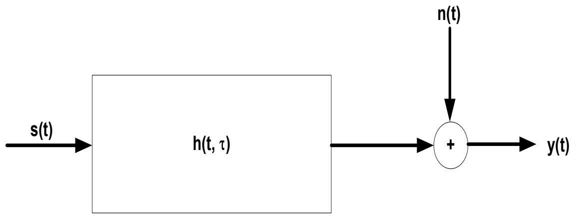

Figure 3.4. The mathematical model of the radio communication

The received signal is the convolution of the *channel* $h(t)$ and the *transmitted signal* $s(t)$.

$$y(t) = \int_{-\infty}^{\infty} s(\tau)h(t-\tau)d\tau + n(t) \tag{3.3}$$

where $s(t)$ is the transmitted signal and $n(t)$ is the complex-valued additive noise.

By using (3.4), and assuming that the signal $m(t) = \mathbb{R}(s(t)e^{j2\pi f_0 t})$ is transmitted through the channel (here $s(t)$ is any low-pass signal and f_0 is the carrier frequency), the received signal is

$$y(t) = \mathbb{R}(\psi(t)\exp^{j2\pi f_0 t}) \tag{3.4}$$

where

$$\psi(t) = \sum_{k=0}^{P-1} b_k s(t-\tau_k)e^{j\theta_k} + n(t) \tag{3.5}$$

Thus, each kth multipath signal component undergoes a time delay τ_k. The mathematical model of the communication is given in Figure 3.4.

3.2.2. Power Delay Profile and Related Parameters of the Multipath Radio Channel

The multipath channel parameters are observed from the power delay profile which is the average of instantaneous power delay profile measurements over a local area. The instantaneous multipath power delay profile of the channel is given by [15]

$$|y(t_0)|^2 = \sum_{k=0}^{P-1} b_k^2(t_0) \tag{3.6}$$

where $y(t)$ is the output of the channel and t_0 is a time instant.

Depending on whether the transmitter and the receiver directly see each other, measured radio channel profiles in different locations of a building are categorized as LOS (Line-of-Sight) and OLOS (Obstructed Line-of-Sight). For each of those categories, the performance of a wireless communication system shows significant variations. Several copies of the transmitted signal arrive at the receiver. These copies may consist of a line-of-sight (LOS) ray and several other rays reflected from or scattered by objects in the environments such as walls, ceilings, tables, etc., which are called non-line-of-sight (NLOS) waves. It is possible that the LOS waves may be attenuated so that they cannot be detected at the receiving-end. The multipath components are added according to their relative arrival times, amplitudes, and phases, and their random envelop sum is observed by the receiver [6]. The shape and the structure of the building, and the resolution of the measurement setup determine the number of detected paths.

The most crucial stage of the location estimation applications is the accurate detection of the direct line-of-sight (DLOS) path between the sender and receiver. The DLOS path represents the straight line between the communicating pair even if there are obstructions between them. The significance of the DLOS path is that the distance between the sender and receiver is readily obtained from TOA or AOA information, therefore any inaccuracy in the estimation of TOA or AOA leads to the wrong position estimates. Also the communication bandwidth has effect on the accuracy of a positioning system. If a system uses TOA for location estimation, it requires wide bandwidths to resolve multipath components and detect the TOA of first path.

From the receiver's point of view, channel profiles are divided into three groups:

[7]:

- DDP (Dominant Direct Path): In this category, the DLOS path is detectable and it is the strongest path in the channel profile. GPS uses TOA for outdoor applications where multipath components are much weaker than the DLOS path.
- NDDP (Non-Dominant Direct Path): Here the measurement system can detect the DLOS path, however it is not the strongest one. GPS receivers that want to lock to the strongest path will inaccurately estimate the TOA which will lead to the positioning error. In such a case, RAKE receiver can resolve the multipath and provide accurate TOA estimation of DLOS path.
- UDP (Undetected Direct Path): The DLOS path is completely undetectable. GPS and RAKE receiver cannot determine the DLOS path in this case.

The estimation error of TOA or DOA of the DLOS path directly affects the performance of the geolocation application. The environmental noise, the signal bandwidth, possible interference from other systems, and the relative power and delay of the signal arriving via other paths contribute to the estimation error of the distance between the sender and receiver.

In Figure 3.5, Figure 3.6, and Figure 3.7, three measured power delay profiles of different indoor multipath channels for respectively DDP, NDDP, and UDP cases are given [9]. The relative received power is on axes y and excess delay is on axes x. The vertical dashed line is the expected delay of the first arriving path (TOA).

There are several so-called channel sounding methods developed for obtaining power delay profile of multipath channels in the literature such as *direct pulse measurements, spread spectrum sliding correlator measurements*, and *swept frequency measurements*. They are not detailed in this study. For further information, we refer to [15].

Different multipath channels are compared and quantified according to the three parameters, namely, *mean excess delay* $\overline{\tau}$, *rms delay spread* σ_τ, and *excess delay spread*

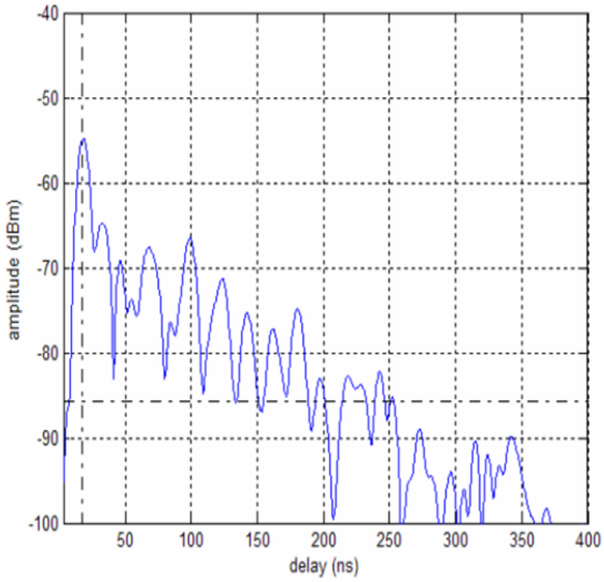

Figure 3.5. A DDP measured power delay profile example

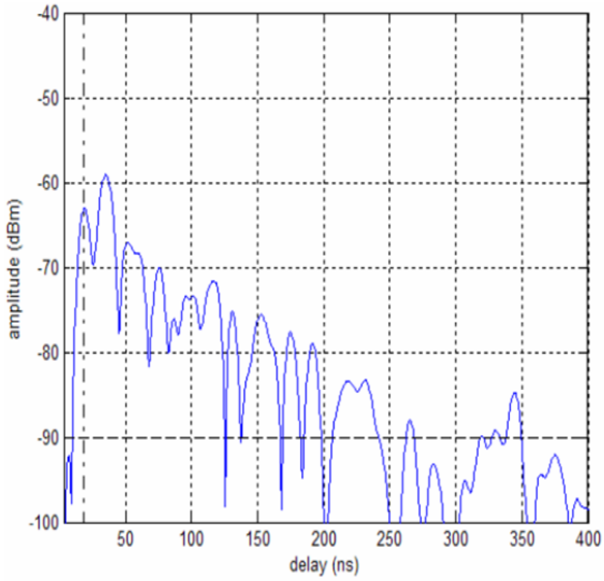

Figure 3.6. A NDDP measured power delay profile example

(X dB) which can be determined from a power delay profile [15].

The first moment of the power delay profile is the mean excess delay and is given by

$$\overline{\tau} = \frac{\sum_k \beta_k^2 \tau_k}{\sum_k \beta_k^2} = \frac{\sum_k P(\tau_k)\tau_k}{\sum_k P(\tau_k)} \tag{3.7}$$

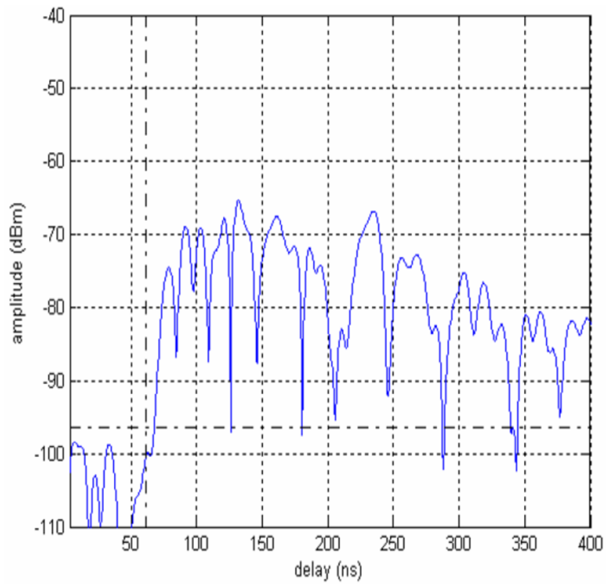

Figure 3.7. A UDP measured power delay profile example

where $P(\tau_k)$ is a single power delay profile which is the temporal average of consecutive impulse response measurements collected and averaged over a local area.

On the other hand, the rms delay spread is obtained from the square root of the second central moment of the power delay profile. It is defined as

$$\sigma_\tau = \sqrt{\overline{\tau_2} - (\overline{\tau})^2} \tag{3.8}$$

where

$$\overline{\tau^2} = \frac{\sum_k \beta_k^2 \tau_k^2}{\sum_k \beta_k^2} = \frac{\sum_k P(\tau_k)\tau_k^2}{\sum_k P(\tau_k)} \tag{3.9}$$

Note that those two parameters define the time dispersive properties of wide band multipath channels. They are obtained from a series of measurements collected from a local area, however, a number of measurements at many local areas are needed in order to properly determine the statistical properties of multipath channel parameters.

Let at time instant τ_x, multipath energy falls X dB below the maximum. In such a case, *excess delay spread* (X dB) of the power delay profile is defined as $\tau_x - \tau_0$, where

τ_0 is the delay of the first arriving signal.

Although power delay profile determines the channel characteristics in time-domain, it is possible to define the channel in frequency-domain by magnitude frequency response. One can be obtained from the other via Fourier transform. For the frequency-domain characterization of a multipath channel, the so-called *coherence bandwidth* is used. It is inversely proportional to the *rms delay spread*.

The small-scale fading can be classified based on either time-delay spread or Doppler spread, however, in this study, it is assumed that indoor radio channel and communicating entities are static, therefore, the classification based on the first parameter is mentioned here. The multipath channel fading can be either flat or frequency-selective depending on the time-delay spread. In flat-fading, the radio channel has a constant gain and linear phase response over a bandwidth which is larger than of the transmitted signal. In such a channel, the gain of the received signal may change in time, however, its spectrum does not. This kind of channel is easy to model and assumed as not having excess delay. On the other hand, if the channel bandwidth which has constant gain and linear phase is smaller than the bandwidth of transmitted signal, it creates frequency-selective fading on the signal. In such a radio channel, several replicas of the original signal which are attenuated and delayed arrive at the receiver. The spectrum of the transmitted signal is distorted. It is not easy to model the frequency-selective fading channels because each multipath component must be modelled. For the analysis of frequency-selective fading channels generally 2-ray Rayleigh fading model, computer generated impulse responses, or measured impulse responses are used.

3.2.3. The Distribution of Multipath Fading

In an indoor wireless radio channel, multipaths cannot be resolved as distinct pulses if the difference in time delay of a number of paths is much less than the reciprocal of the transmission bandwidth. The unresolvable paths add vectorially and the envelope of their sum is observed. Thus, the envelope is a random variable. Suppose that B is the transmission bandwidth. If $t_{k_i} - t_{k_j} \leq 1/B, \;\; i,\, j = 1, 2, ..., n$, then

$$b_k e^{j\theta_k} = \sum_{i=1}^{n} b_{k_i} e^{j\theta_{k_i}} \tag{3.10}$$

defines the resolved multipath component.

The distribution of the amplitude of multipaths may vary depending on the area, objects in the environment, etc. In this section, two of the well known multipath amplitude distributions are given.

3.2.3.1. The Rayleigh Distribution. If there is no strong received component, the small-scale amplitude fluctuations are well modeled by the Rayleigh fading with a probability density function (pdf) given by

$$f(x) = \frac{x}{\sigma^2} \exp \frac{x^2}{2\sigma^2} \tag{3.11}$$

where σ is the Rayleigh parameter. It is also called the most probable value. $\sqrt{\pi/2}\sigma$ and $(2 - \pi/2)\sigma^2$ the mean and the variance of the distribution, respectively.

The theoretical definition of the Rayleigh distribution is done by Clarke's model used for mobile channel [6]. This model assumes that the transmitted signal arrives the receiver via P directions, the ith path has a complex strength $x_i e^{j\theta_i}$ and can be described by a phasor with an envelope x_i and a phase θ_i. At the receiving-end, these signals are added vectorially and the resultant phasor is given by

$$x e^{j\theta} = \sum_i x_i e^{j\theta_i} \tag{3.12}$$

According to Clarke's model, over small areas and in the absence of LOS path, the x_i's are almost equal ($x_i = x, i = 1, 2, ..., P$). Thus, (3.12) becomes $x e^{j\theta} = x \sum_i e^{j\theta_i}$. The phase of each path θ_i depends on the path length, and changes by 2π when the path length changes by a wavelength. Thus, phases are uniformly distributed over $[0, 2\pi)$. Now, the problem is to obtain the distribution of the envelope sum of a large number of sinusoids with constant amplitude and uniformly-distributed random phases. The In-phase and Quadrature (I and Q) components of the received signal are independent, and, by the central limit theorem, are Gaussian random variables. The joint distribution of x ($x = \sqrt{I^2 + Q^2}$) and θ ($\theta = \arctan(Q/I)$) was studied by Rayleigh [6] and his research revealed that x and θ are independent, x is Rayleigh and θ is uniformly distributed random variables.

Slack shows that even when there are only six *sine* waves with uniformly distributed and independently fluctuating phases are combined, the resulting amplitude and phase are very closely Rayleigh and uniformly distributed, respectively [6].

As stated before, it is assumed that x_i's are equal, however it is not realistic because it means that each path has the same attenuation. On the other hand, it can be shown that even when the amplitudes of multipaths are not equal and any single one of them does not contribute a major fraction of the received power (i. e. , $x_i << \sum x_i^2$, $i = 1, 2, ..., P$), the variations of the resulting amplitude can be described by Rayleigh distribution.

In the literature, there are lots of studies based on measurement data showing that the Rayleigh distribution is suitable for modelling the indoor radio channel and small scale fading. Also the Rician distribution can describe some LOS paths. On the other hand, the log-normal distribution is used when only signal levels below the median are considered. [2] investigated the amplitudes of the multipath components in a factory environment based on measurement data. It has been shown that the amplitude has Rayleigh distribution. On the other hand, measurement data collected in an office environment show that the amplitude distribution is approaching to Rayleigh than log-normal [6]. According to measurement data collected in a scenario where either receiver or transmitter is located outside the building, and the other inside, the amplitude has showed a good Rayleigh distribution [6]. When both receiver and transmitter are inside building, measurements show that the multipath channel coefficients can be modelled as Rayleigh [6]. Depending on the presence or absence of a LOS path, Rician distributions can be used as well.

3.2.3.2. The Rician Distribution. When there is a strong path in the environment apart from low level scattered paths, the Rician distribution can be used to model it. This strong path can be either a LOS path or a path that goes through much less attenuation compared to other received components. This path was called *fixed path* by Turin [6]. As a result, the received signal vector can be assumed to be the sum of two vectors; a vector which has deterministic amplitude and phase, that is, the fixed path, and a scattered Rayleigh vector whose amplitude and phase are random. Let pe^{jq} be the random component, with p being Rayleigh and q being uniformly distributed and ue^{jv} be the fixed component where u and v are not random. The received signal vector $xe^{j\theta}$ is the phasor sum of the aforementioned two signals. Rice has showed that the joint pdf of x and θ is given by [6]

$$f(x,\theta) = \frac{x}{2\pi\sigma^2} \exp - \frac{x^2 + u^2 - 2xu\cos(\theta - v)}{2\sigma^2} \tag{3.13}$$

where $x \geq 0$, $-\pi \leq (\theta - \beta) \leq \pi$.

Since the length and phase of the fixed path usually changes, v can be said to be a uniformly distributed random variable over $[0,2\pi)$. This assumption leads to the independency between x and θ. As a result, x can be modeled as Rician distribution and its pdf is given by

$$f(x) = \frac{x}{\sigma^2} \exp(\frac{-x^2 + u^2}{2\sigma^2}) I_0(\frac{xu}{\sigma^2}) \tag{3.14}$$

where I_0 is the *zero*th-order modified Bessel function of the first kind, u is the envelope of the strong component and σ^2 is proportional to the power of the Rayleigh component.

As it can be seen in (3.14), if u approaches to zero, the strong path is eliminated and the amplitude distribution becomes Rayleigh. As a result, Rician distribution includes Rayleigh distribution as a special case.

4. PROBLEM STATEMENT

In this section, the TOA estimation with MUSIC under non-Gauss noise which is modelled by the stable distribution family is presented. Before going through the proposed solution, it is worthy to give information about TOA estimation with MUSIC under Gauss noise.

4.1. TOA Estimation with MUSIC under Gauss Noise

Although IFT have been used for years for the estimation of time delay characteristics of multipath radio channels, super-resolution methods have been getting more popular in recent years due to the fact that they provide better resolution than IFT [16].

In [16], the TOA estimation problem under Gaussian noise is analyzed and second-order-statistics (SOS) based MUSIC was proposed in order to resolve multipaths of indoor radio channel. First of all, frequency-domain data is obtained, and autocorrelation matrix is estimated from the observed data. The MUSIC is based on the eigen-decomposition of the autocorrelation matrix. It is applied to the second-order-statistics of the data and the MUSIC pseudospectrum whose peaks give the path delays of the radio channel is obtained. Also, time-diversity technique is applied to the problem to improve the accuracy of the TOA estimate. At each diversity branch of receiver, the TOA is estimated independently, and the estimates coming from all branches are combined to attain an optimum estimate. There are various combining algorithms for different diversity techniques. The equal-gain combining algorithm is used in [16]. The MUSIC, IFT and DSSS are applied to the measured frequency-domain data and it is shown that the SOS-MUSIC provides the best performance.

4.2. TOA Estimation with MUSIC under non-Gauss Noise

The complex low pass equivalent of the multipath indoor radio channel impulse response is given by

$$h(t) = \sum_{k=0}^{P-1} b_k \delta(t - \tau_k) \tag{4.1}$$

where P is the number of multipath components, $b_k = |b_k| e^{j\theta_k}$ and τ_k are the complex attenuation and propagation delay of the kth path, respectively. Let τ_k's be in the increasing order. Therefore, τ_0 is the first arriving path that needs to be estimated for indoor positioning purposes. Also, note that b_k is complex Gaussian and θ_k is uniformly distributed between $[0, 2\pi)$, that is, $|b_k|$ is Rayleigh distributed. By taking the Fourier transform of (4.1), the frequency domain channel response is obtained as follows

$$H(f) = \sum_{k=0}^{P-1} b_k e^{-j2\pi f \tau_k} \tag{4.2}$$

If we exchange the role of time and frequency variables in (4.2), we obtain a harmonic signal model [16]. As a result, any spectral estimation technique suitable for the harmonic signal model is applicable to the frequency response of the multipath indoor radio channel for time-domain analysis [16].

$$H(\tau) = \sum_{k=0}^{P-1} b_k e^{-j2\pi f_k \tau} \tag{4.3}$$

In order to obtain discrete frequency data, the M-point DFT is applied to the (4.1). The discrete channel frequency response $H(f)$ has M coefficients at M equally spaced frequencies. Δf is the frequency increment. The resulting equation is given by

$$H(m\Delta f) = \sum_{k=0}^{P-1} b_k e^{-j2\pi (f_0 + m\Delta f)\tau_k} \tag{4.4}$$

where $m = 0, 1, \ldots, M-1$. The channel is assumed to be low-pass, therefore $f_0 = 0$.

By taking into account noise in the environment which is assumed to be complex isotropic $S\alpha S$ distributed random process, the sampled discrete frequency domain channel response is given by

$$x(m) = H(m\Delta f) + n(m) = \sum_{k=0}^{P-1} b_k e^{-j2\pi m\Delta f\tau_k} + n(m) \tag{4.5}$$

The vector form of the signal is

$$\mathbf{x}\mathbf{=}\mathbf{H}\mathbf{+}\mathbf{n}\mathbf{=}\mathbf{A}\mathbf{s}\mathbf{+}\mathbf{n} \tag{4.6}$$

where

$\mathbf{x} = [x(0) \quad x(1) \quad \ldots \quad x(M-1)]^T$

$\mathbf{H} = [H(0) \quad H(\Delta f) \quad \ldots \quad H((M-1)\Delta f)]^T$

$\mathbf{n} = [n(0) \quad n(1) \quad \ldots \quad n(M-1)]^T$

$\mathbf{A} = [\mathbf{a}(\tau_0) \quad \mathbf{a}(\tau_1) \quad \ldots \quad \mathbf{a}(\tau_{P-1})]$

$\mathbf{a}(\tau_k) = [1 \quad e^{-j2\pi\Delta f\tau_k} \quad e^{-j2\pi 2\Delta f\tau_k} \quad \ldots \quad e^{-j2\pi(M-1)\Delta f\tau_k}]^T$

$\mathbf{s} = [b_0 \quad b_1 \quad \ldots \quad b_{P-1}]^T$

and T denotes the transpose operation.

It is worthy to define the $M \times P$ $\mathbf{A}$ matrix for clarity.

$$\mathbf{A} = \begin{bmatrix} 1 & 1 & . & . & 1 \\ e^{-j2\pi\Delta f\tau_0} & e^{-j2\pi\Delta f\tau_1} & . & . & e^{-j2\pi\Delta f\tau_{P-1}} \\ e^{-j2\pi2\Delta f\tau_0} & e^{-j2\pi2\Delta f\tau_1} & . & . & e^{-j2\pi2\Delta f\tau_{P-1}} \\ . & . & . & . & . \\ . & . & . & . & . \\ e^{-j2\pi(M-1)\Delta f\tau_0} & e^{-j2\pi(M-1)\Delta f\tau_1} & . & . & e^{-j2\pi(M-1)\Delta f\tau_{P-1}} \end{bmatrix} \tag{4.7}$$

Generally, MUSIC is applied to the covariance matrix for the separation of signal and noise subspaces. However, due to infinite variance of the complex isotropic $S\alpha S$ noise, the covariance is not valid. Instead, the so-called *FLOM-based covariation matrix* is calculated from data matrix and used as the input to the MUSIC. The overall method is called *FLOM-MUSIC TOA estimator.* The step-by-step derivation of TOA estimation algorithm with FLOM-MUSIC under stable noise is given in the following section.

Before presenting the solution, the model of the channel and noise signals must be determined. In [13], the ROC-MUSIC algorithm for source localization in impulsive noise environments is presented and it is assumed that both signal and noise are jointly complex isotropic $S\alpha S$ with characteristic exponent $\alpha \in (1, 2]$. However, information signals always have finite variance, and therefore, the assumption made by [13] about the bearing signals is not realistic [14].

In this thesis, the channel and the environmental noise are assumed to be complex Gaussian and complex isotropic $S\alpha S$ with $\alpha \in (1, 2]$, respectively. As mentioned in Chapter 2, second order statistics cannot be applied to the TOA estimation problem due to the impulsive noise assumption. Instead, FLOMs will be used and the resulting covariation matrix will be called *FLOM-based covariation matrix* [14].

The assumptions made for the derivation of the solution are as follows:

- **A1**: In $b_k = |b_k|e^{j\theta_k}$, the amplitude $|b_k|$ and the phase θ_k are statistically independent real random variables. The first is Rayleigh distributed while the latter is a sequence of i.i.d. random variables with uniform distribution over $[0, 2\pi)$.

- **A2**: n_m is the sequence of zero-mean, i.i.d. complex isotropic $S\alpha S$ random variables with $1 < \alpha \leq 2$.
- **A3**: $\mathbf{A}$ given by (4.7) is of full rank. This assumption is necessary for all subspace methods in order to extract the desired information from noise.

Note that, from **A2** and **A3**, $\mathbf{x}$ given by (4.6) is zero-mean.

Now, the task is to construct the FLOM-based covariation matrix $\mathbf{C}$ from N snapshots of data and apply MUSIC to seperate the signal and noise subspaces by eigen-decomposition. The proposed solution for the TOA estimation under impulsive noise is given in the next section.

4.2.1. TOA Estimation with FLOM-MUSIC

The step-by-step derivation of the problem solution is as follows:

1) Build data matrix from N data snapshots. Each snapshot has length of M. Resulting data matrix is $M \times N$.

2) Obtain the $(M \times M)$ FLOM-based covariance matrix, $\mathbf{C}$ which will be the input for MUSIC algorithm introduced in the third step. The covariance matrix $\mathbf{C}$ is computed as follows [14]

$$\mathbf{C} = (1/\mathrm{N})(\mathbf{X}|\mathbf{X}^*|^{(\mathrm{p}-2)}\mathbf{X}^*); \tag{4.8}$$

3) The conventional MUSIC under Gauss noise is based on the eigen-decomposition of the correlation matrix. However, α-stable random processes do not have finite pth order moment for $p \geq \alpha$. Instead of correlation matrix, FLOM-based covariation matrix $\mathbf{C}$ is defined in the second step. Now, the input of the MUSIC is the FLOM-based covariation matrix, $\mathbf{C}$. As a result of eigen-analysis of $\mathbf{C}$, the following equation is obtained

$$\mathbf{C} = \mathbf{PDP}^{-1} \tag{4.9}$$

where $\mathbf{D}$ is the $(N \times N)$ diagonal matrix having eigenvalues of $\mathbf{C}$ on the diagonal, and $\mathbf{P}$ is the $(N \times N)$ matrix composed of N eigenvectors on the columns. It can be readily seen that each eigenvector has a length of N.

The matrix form of $\mathbf{C}$ is given as follows

$$\mathbf{C} = \mathbf{ASA} + \gamma\mathbf{I} \tag{4.10}$$

The FLOM-based covariation matrix $\mathbf{C}$ has the following properties [14]

- It is bounded except for $\alpha < 1$ which implies a high impulsive environment. For such a condition, zero-memory nonlinearity (ZMNL) is proposed to clip the undesired impulsive noise [14].
- It has the TOA information embedded in $\mathbf{A}$.
- The elements on the diagonal of $\mathbf{C}$ are identical.
- $\mathbf{S}$ in (4.10) is nonsingular.

Assuming that $N > P$, theoretically the $N - P$ smallest eigenvalues of $\mathbf{C}$ are all equal to the dispersion γ. The eigenvectors corresponding to $N - P$ smallest eigenvalues of $\mathbf{C}$ are called noise eigenvectors, while the P largest eigenvectors are called signal eigenvectors. What MUSIC does is that it splits N-dimensional subspace that contains signal contaminated by complex isotropic SαS noise into two orthogonal subspaces, called signal subspace and noise subspace spanned by the signal eigenvectors and noise eigenvectors, respectively.

Let

$$\mathbf{J} = [\mathbf{j}_0 \quad \mathbf{j}_1 \quad \ldots \quad \mathbf{j}_{P-1}] \tag{4.11}$$

be the signal eigenvectors and

$$\mathbf{K} = [\mathbf{k}_P \quad \mathbf{k}_{P+1} \quad \ldots \quad \mathbf{k}_{N-1}] \tag{4.12}$$

be the noise eigenvectors.

The projection matrix of the noise subspace is determined by

$$\Phi = \mathbf{K}(\mathbf{K}^H\mathbf{K})^{-1}\mathbf{K}^H = \mathbf{K}\mathbf{K}^H \tag{4.13}$$

Due to the fact that $\mathbf{a}(\tau_k)$, $(k = 0, 1, \ldots, P-1)$, must be in the signal subspace

$$\Phi\mathbf{a}(\tau_k) = 0. \tag{4.14}$$

As a result, the multipath delays τ_k, $0 < k < P-1$, are obtained from the peaks of the MUSIC pseudospectrum given by

$$S_{MUSIC} = \frac{1}{\mathbf{a}^H(\tau)\mathbf{K}\mathbf{K}^H\mathbf{a}} = \frac{1}{\sum_{i=P}^{N-1} |\mathbf{k}_i\mathbf{a}|^2} \tag{4.15}$$

The first peak of the pseudospectrum is the estimate of τ_0 denoted by $\widehat{\tau}_0$. Once it is estimated, the distance between the transmitter and the receiver are readily calculated. The S_{MUSIC} pseudospectrum gives the delay characteristics of the indoor radio channel, that is, the arrival times of the multipath components, however, power levels on the pseudospectrum are not realistic, therefore, MUSIC does not give a complete characterization of the channel. Whereas $\widehat{\tau}_0$ is the TOA of the first arriving path, other delays stem from other multi paths.

The derivation is done for non-Gaussian distributed noise. IFT is a conventional method for finding the delay characteristics of a multipath radio channel. Under Gauss noise, the TOA estimation with SOS-based MUSIC was studied and compared to IFT in [16] and it was shown that SOS-MUSIC is superior to IFT, that is, IFT cannot resolve multipath especially for low SNR values. Due to the fact that non-Gauss noise is more disruptive than Gauss noise, it is apparent that IFT would be completely unsatisfactory under impulsive noise for low GSNR values, therefore, it was not considered in our study.

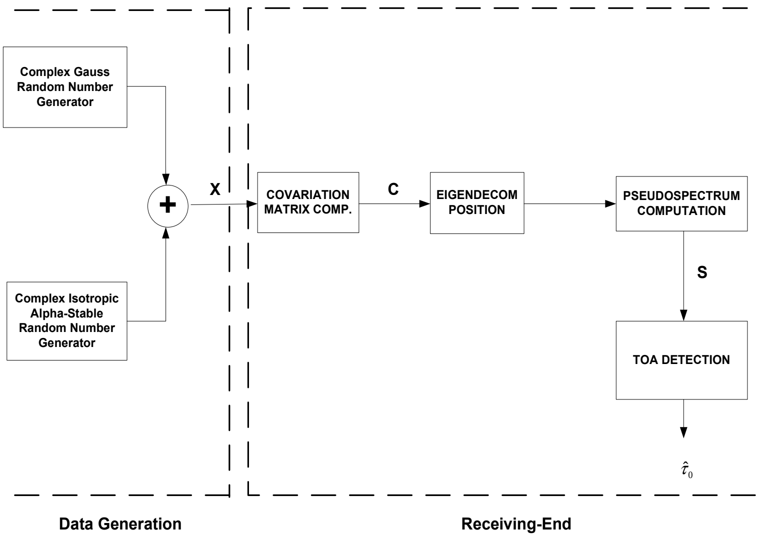

Figure 5.1. Simulation Process

5. SIMULATION RESULTS

In this chapter, the performance of the proposed FLOM-MUSIC TOA estimation algorithm is evaluated and compared with the performance of SOS-MUSIC TOA estimator [16] under non-Gaussian noise. The effect of the GSNR (Generalized Signal-to-Noise Ratio), the characteristic exponent α, and the fractional lower order moment p on the estimators' performances are studied. Also, the distributions of FLOM-MUSIC and SOS-MUSIC TOA estimators are interpreted via the Kolmogorov-Smirnov goodness of fit test [1]. Figure 5.1 picturies the estimation process based on computer simulations. The observed data vector is obtained by sampling the channel frequency response uniformly over a given frequency band as given in (4.5). For indoor multipath channels, it can be assumed that the maximum delay τ_{max} is less than 500 nsec [7]. Therefore, the frequency sampling interval Δf is chosen to be $1/2\tau_{max} = 1$ MHz. The bandwidth is chosen to be 100 MHz, therefore the size of one snapshot is $f_s/\Delta f = 2B/\Delta f = 200$ where f_s is the sampling frequency. Due to the low-pass assumption, it is assumed that the carrier frequency $f_0 = 0$ in (4.4).

Due to the infinite variance of α-stable random processes, the traditional signal-to-noise ratio (SNR) definition is invalid in this study. Instead, so called the generalized

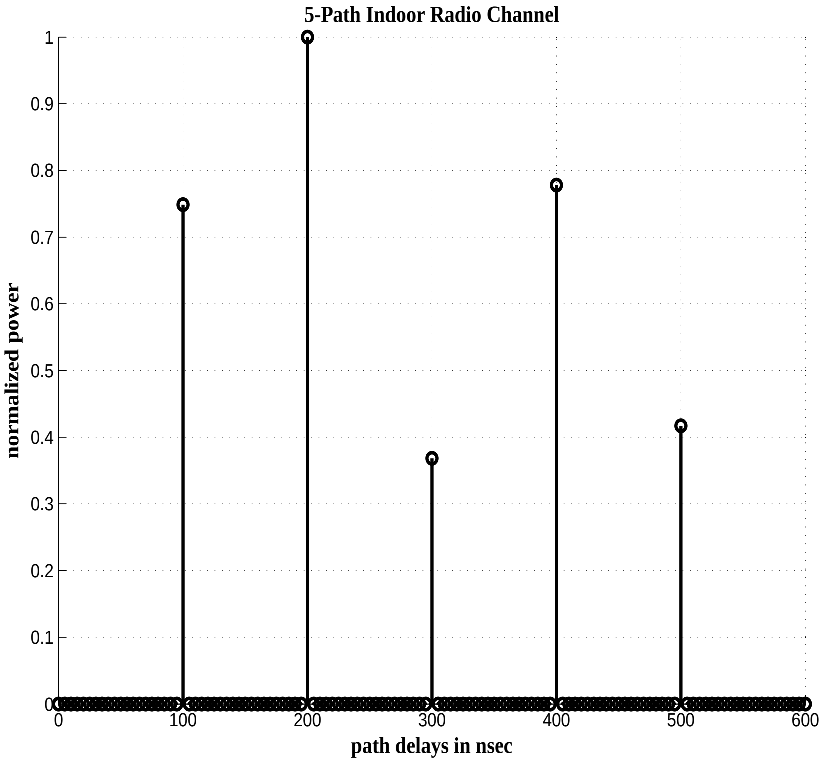

Figure 5.2. 5-path indoor radio channel sample

signal-to-noise ratio (GSNR) [14] is used and defined as follows:

$$\mathrm{GSNR} = 10\log(\mathrm{E}\{|h(\mathrm{t})|^2\}/\sigma^\alpha) \tag{5.1}$$

If $\alpha = 2$, (5.1) becomes the well-known signal-to-noise ratio (SNR) that defines the ratio of signal variance to noise variance.

The resulting pseudospectrum of our TOA estimation algorithm has peaks around the delays of the indoor radio channel paths if the estimation is successful. Due to the fact that the pseudospectrum is in time domain, the places of those peaks give the estimates of the path delays. Figure 5.2, Figure 5.3, and Figure 5.4 show a simulated 5-path indoor radio channel and the corresponding FLOM-MUSIC and SOS-MUSIC pseudospectra, respectively. For the rest of our simulations, it is assumed that the indoor radio channel has two paths introducing 100 nsec and 200 nsec delays, respectively. It is also assumed that the channel is complex Gaussian with uniformly distributed phase over $[0, 2\pi)$ rad and the noise is complex isotropic SαS. The parame-

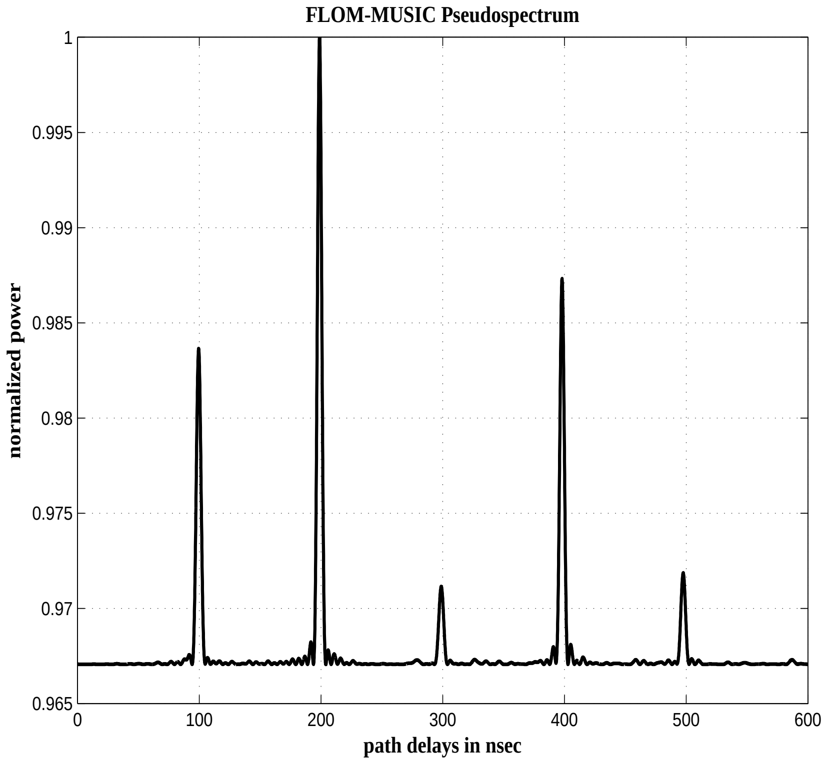

Figure 5.3. The FLOM-MUSIC pseudospectrum

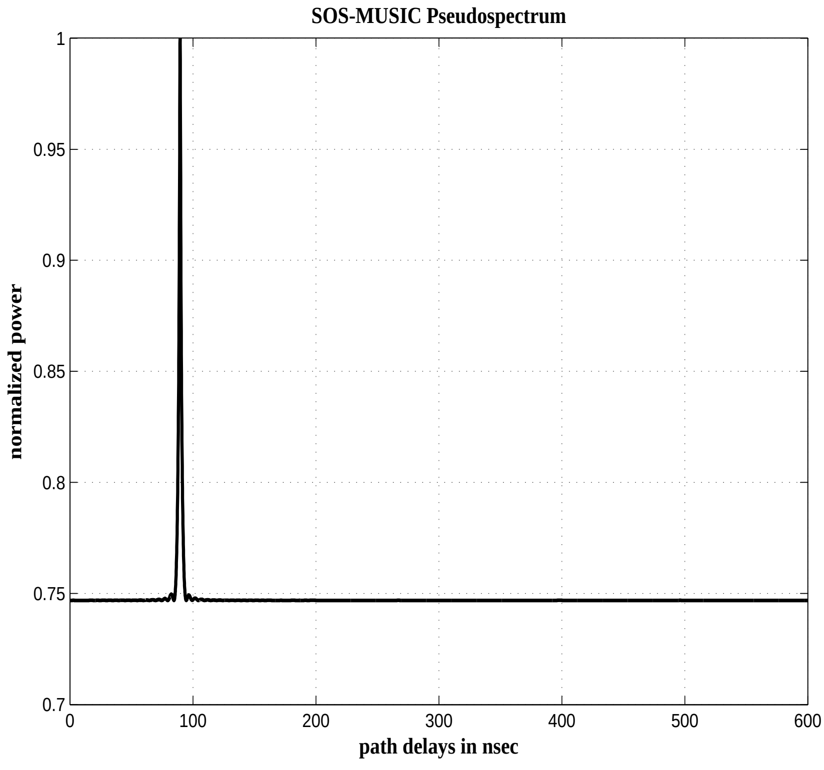

Figure 5.4. The SOS-MUSIC pseudospectrum

ters of the stable noise are assumed to be known although there are several parameter estimation methods for α-stable random processes in the literature [3].

The MUSIC algorithm assumes that the covariation matrix is both Hermitian and Toeplitz which assures that it is conjugate symmetric and has equal elements along all diagonals. However, the sample covariation matrix $\mathbf{C}$ estimated from data samples does not fit this assumption. In order to attain conjugate symmetry, two methods are used and their performances are compared via simulations. Forward-backward method is the first one used in order to improve the FLOM-covariation matrix. The resulting forward-backward covariation matrix is calculated as follows

$$\mathbf{C}^{\mathrm{FB}} = \frac{1}{2}(\mathbf{C} + \mathbf{J}\mathbf{C}^{*}\mathbf{J}) \tag{5.2}$$

where $*$ denotes conjugate and $\mathbf{J}$ is the (M$\times$M) exchange matrix whose elements are zero except for ones on the anti-diagonal. The proposed algorithm using forward-backward method is called FLOM-MUSIC with forward-backward improvement. The second method is the well-known general improvement method given by

$$\mathbf{C}^{\mathrm{G}} = \frac{1}{2}(\mathbf{C} + \mathbf{C}^{*}) \tag{5.3}$$

This method is named as FLOM-MUSIC with general improvement.

In simulations, the performances of FLOM-MUSIC and SOS-MUSIC TOA estimators are evaluated in terms of two criteria; the success rate and the mean-squared-error (MSE) of the first arriving path. The FLOM-MUSIC is the proposed solution while the SOS-MUSIC is the TOA estimation algorithm proposed for Gauss noisy environments [16]. On the other hand, a threshold level must be determined in order to estimate path delays from the pseudospectrum. In other words, peaks having larger power than the threshold power level will be accepted as path delays. In our simulations, for each value of GSNR, α and p, 1000 trials are done and they have taken values between [5 dB,30 dB], [1,2] and [0.5,2], respectively. The total number of simulated trials is 160000, that is, 160000 pseudospectra were obtained. The noise floor of all obtained pseudospectra are almost equal to 57 dB, that is, the minimum power level of each pseudospectra are about 57 dB. It is also seen from the simulated pseudospectra that maximum power level of outliers is 57.184 dB. As a result, it was chosen that peaks having power higher than 57.184 dB (it is equal to the noise floor plus 0.174 dB) which is the threshold level are evaluated as delay estimates. The threshold level should be carefully determined from measurements or simulations. It affects the sensitivity of the receiver.

In our study, the success rate is defined in two different ways as follows:

- The algorithm successfully resolves two paths, that is, the pseudospectrum exhibits exactly two peaks inside the interval [90 nsec,210 nsec]. The powers of those peaks are higher than 57.184 dB. It does not have any peak higher than the threshold level out of that region. It is named as the resolution success rate.
- If the first peak of the resulting pseudospectrum over the threshold is around 100 nsec (in the interval of [90 nsec,110 nsec]), it is assumed that the trial is successful because it gives the TOA. If exist, other peaks are neglected. It can be called as the success rate for finding the TOA.

In both cases, the success rate becomes the ratio, in percentage, of the successful trials to the total number of trials. The successful estimates of two paths are denoted by $\hat{\tau}_0$ and $\hat{\tau}_1$.

The mean-squared-error is the second evaluation parameter which is the averaged sample mean-squared error of the first peak in the pseudospectrum having power larger than 57.184 dB. The location of this peak gives the estimate of τ_0, denoted by $\hat{\tau}_0$. The success of the estimator is not considered for the computation of the MSE. It is calculated as follows:

$$\mathrm{MSE} = (1/\mathrm{R}) \sum_{\mathrm{b}=1}^{\mathrm{R}} (\hat{\tau}_0(\mathrm{b}) - \tau_0)^2 \tag{5.4}$$

where R is the total number of trials.

Under impulsive noise, 1000 trials are performed and the success rates and the MSE of the general and forward-backward FLOM-MUSIC and SOS-MUSIC are computed for each GSNR, α, and p values. During each trial, the data matrix is built from 100 snapshots and each snapshot is a 200-point vector. The resulting pseudospectrum is evaluated at 10000 points.

5.1. The Effect of the GSNR on the Performances of FLOM-MUSIC and SOS-MUSIC

As stated before, the traditional SNR definition is invalid for impulsive noise due to its infinite variance. Instead, GSNR given by (5.1) is used. It is changed over [5 dB,30 dB] and for each GSNR value, 1000 trials are done for specific characteristic exponent α and fractional moment order p values. For each trial, it is determined if the estimators resolve two paths successfully, if they have a peak around 100 nsec and the MSE of the first peak over the threshold level is calculated.

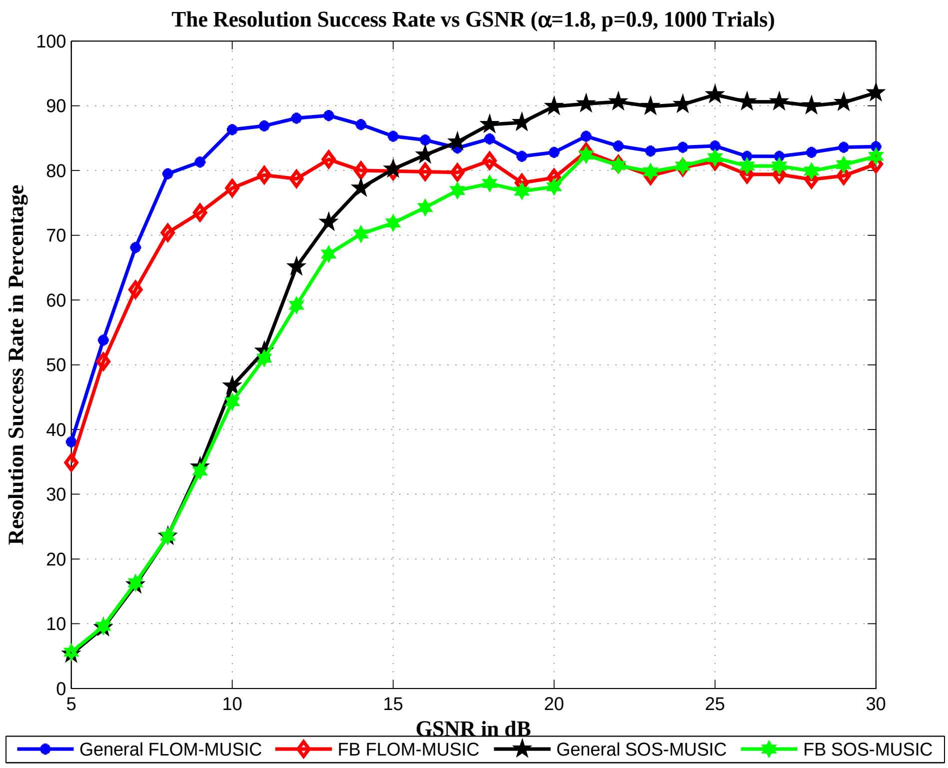

Figure 5.5. Resolution Success rate vs GSNR for $\alpha = 1.8$ and $p = 0.9$

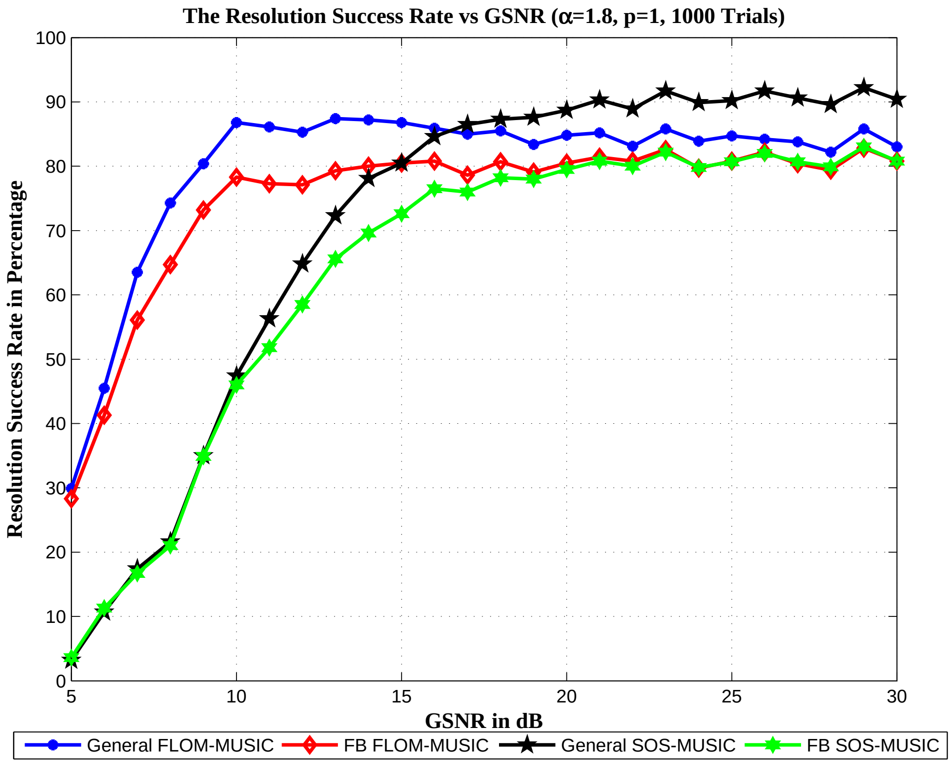

Figure 5.6. Resolution Success rate vs GSNR for $\alpha = 1.8$ and $p = 1$

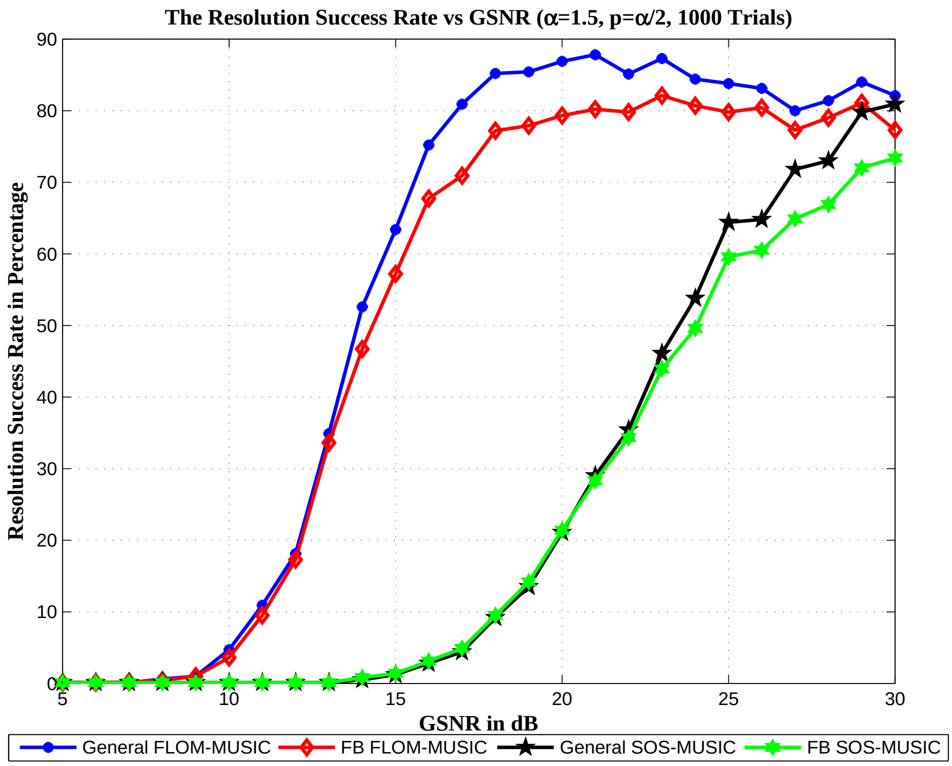

Figure 5.7. Resolution Success rate vs GSNR for $\alpha = 1.5$ and $p = 0.75$

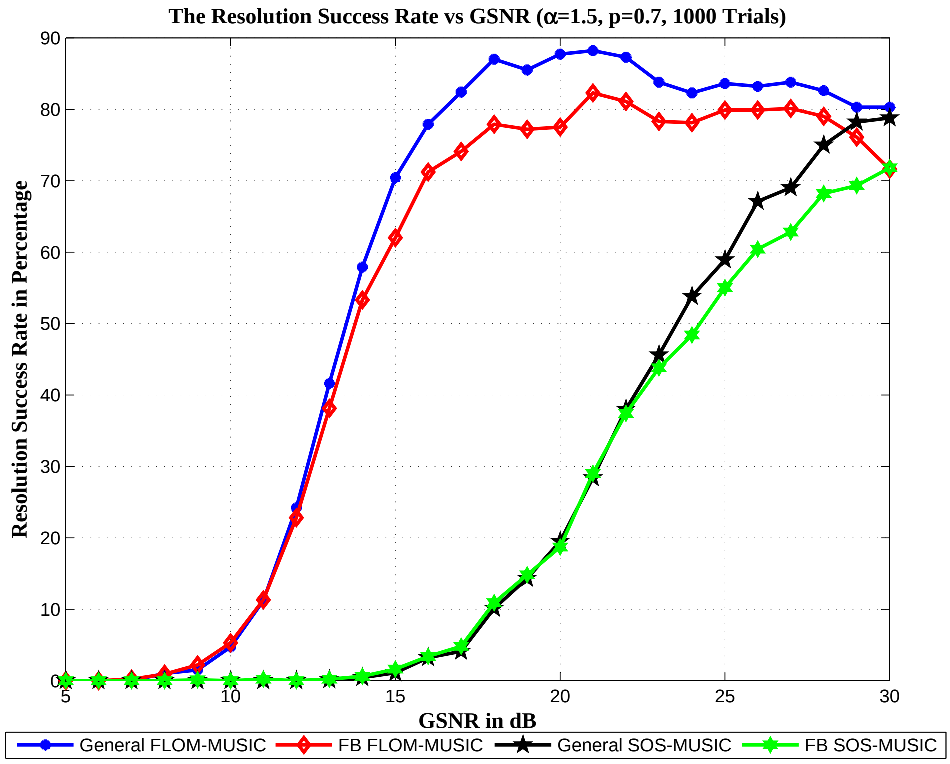

Figure 5.8. Resolution Success rate vs GSNR for $\alpha = 1.5$ and $p = 0.7$

The resolution success rates for the general FLOM-MUSIC, the forward-backward FLOM-MUSIC, the general SOS-MUSIC, and the forward-backward SOS-MUSIC are presented in Figure 5.5, Figure 5.10, Figure 5.7, and Figure 5.8. In the literature, the noise with the characteristic exponent $\alpha = 1.8$ is referred to as slightly impulsive whereas stable noise with $\alpha = 1.5$ is called highly impulsive [14]. For low GSNR values, the general FLOM-MUSIC is the most successful while forward-backward SOS-MUSIC gives the worst performance. The superior performance of the general FLOM-MUSIC gets more apparent under $\alpha = 1.5$. Although the general SOS-MUSIC provides slightly better performance than the general FLOM-MUSIC under $\alpha = 1.8$, it cannot reach the same resolution success rate with that of the general FLOM-MUSIC as α decreases even under maximum GSNR value equals to 30 dB.

In Figure 5.9, Figure 5.10, Figure 5.11, and Figure 5.12, simulation results for the second successful estimate definition are given. Here, each trial having the first peak with larger power than the threshold level inside [90 nsec,110 nsec] are assumed to be successful. The success rate values are higher than the resolution success rate values for the same GSNR.

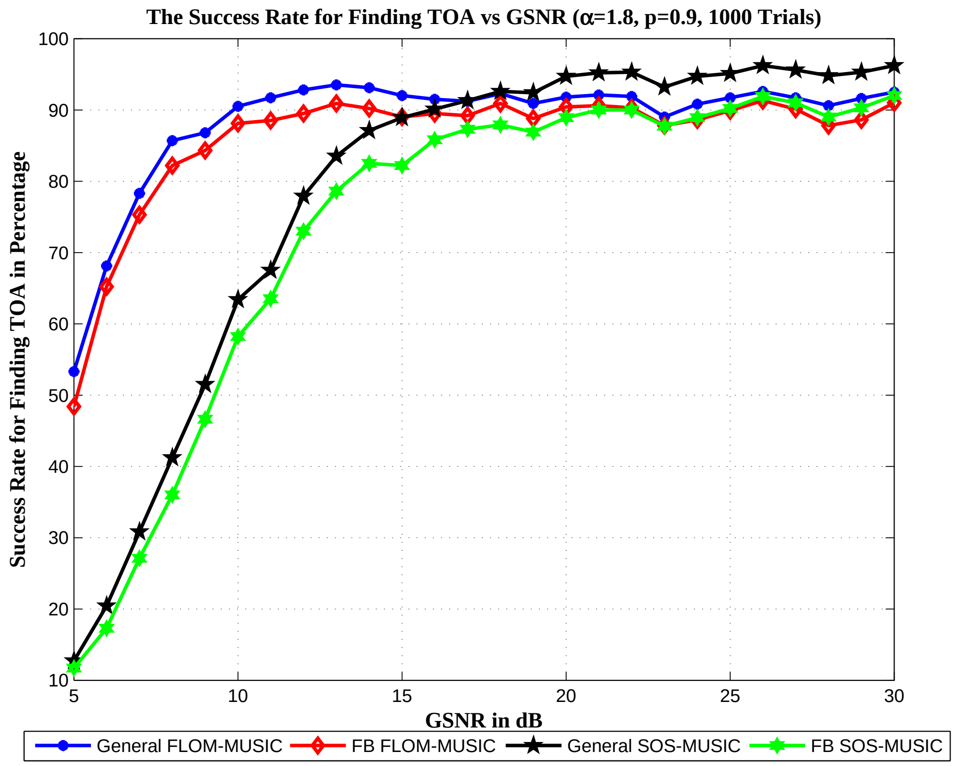

Figure 5.9. Success rate for finding TOA vs GSNR for $\alpha = 1.8$ and $p = 0.9$

The error on the estimates is a significant parameter for the evaluation of the estimators. As seen in Figure 5.13, Figure 5.14, Figure 5.15, and Figure 5.16, for low GSNR values, forward-backward FLOM-MUSIC and SOS-MUSIC have smaller estimation errors than general FLOM-MUSIC and SOS-MUSIC. However, by increasing GSNR, the estimators with general improvement provide lower estimation errors than the estimators with forward-backward improvement. Another result is that MSE is higher for lower α.

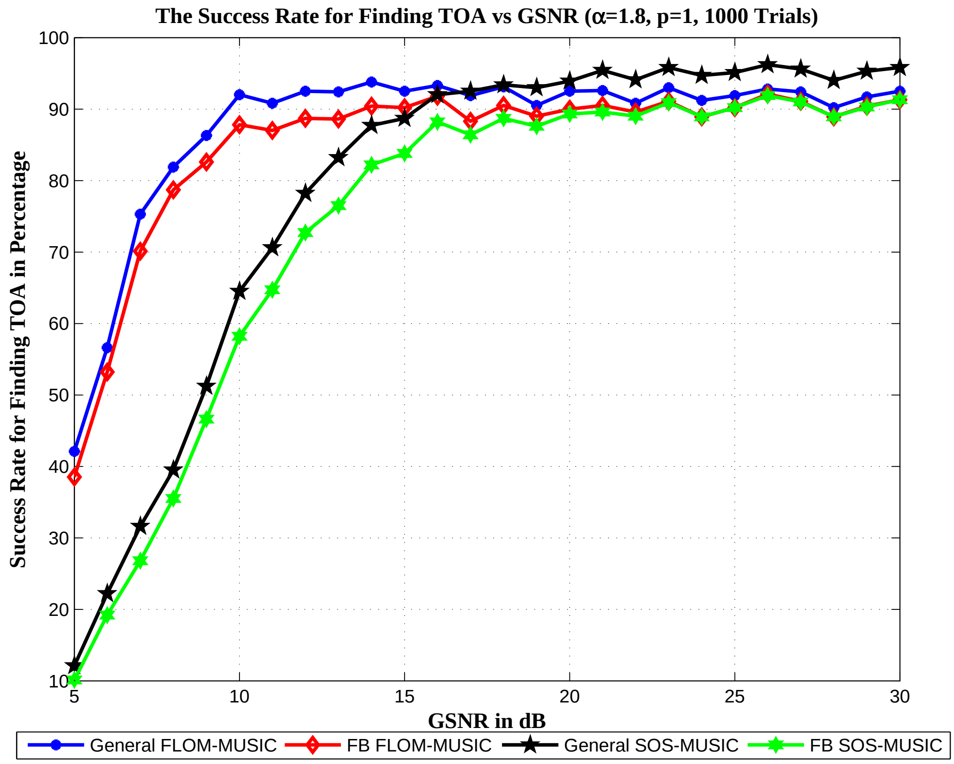

Figure 5.10. Success rate for finding TOA vs GSNR for $\alpha = 1.8$ and $p = 1$

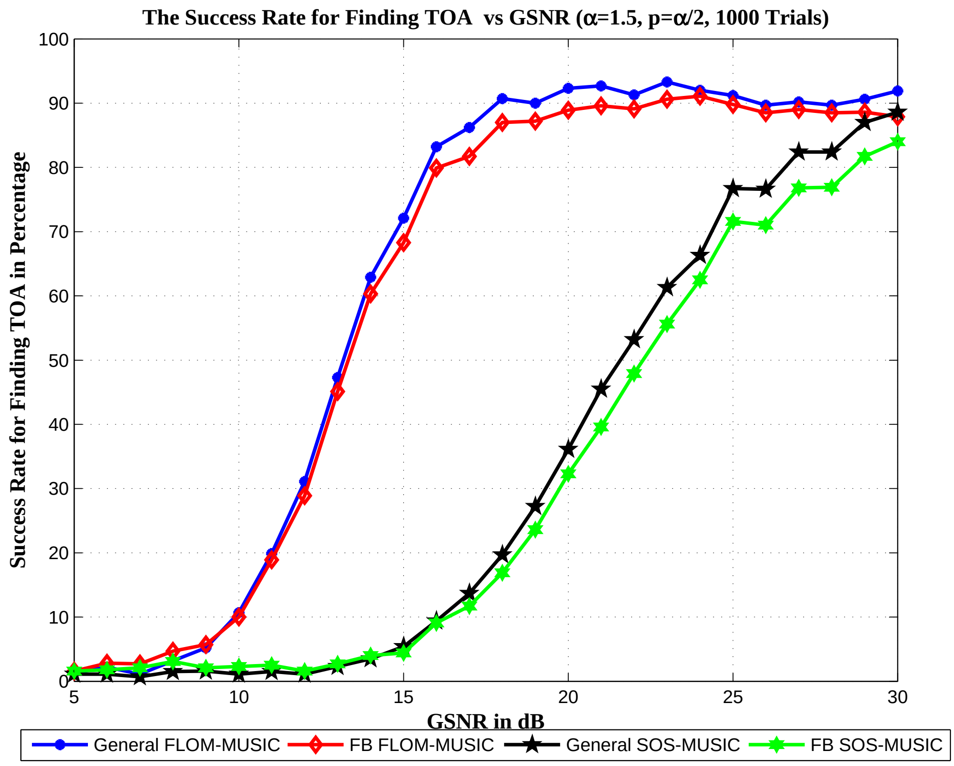

Figure 5.11. Success rate vs GSNR for $\alpha = 1.5$ and $p = 0.75$

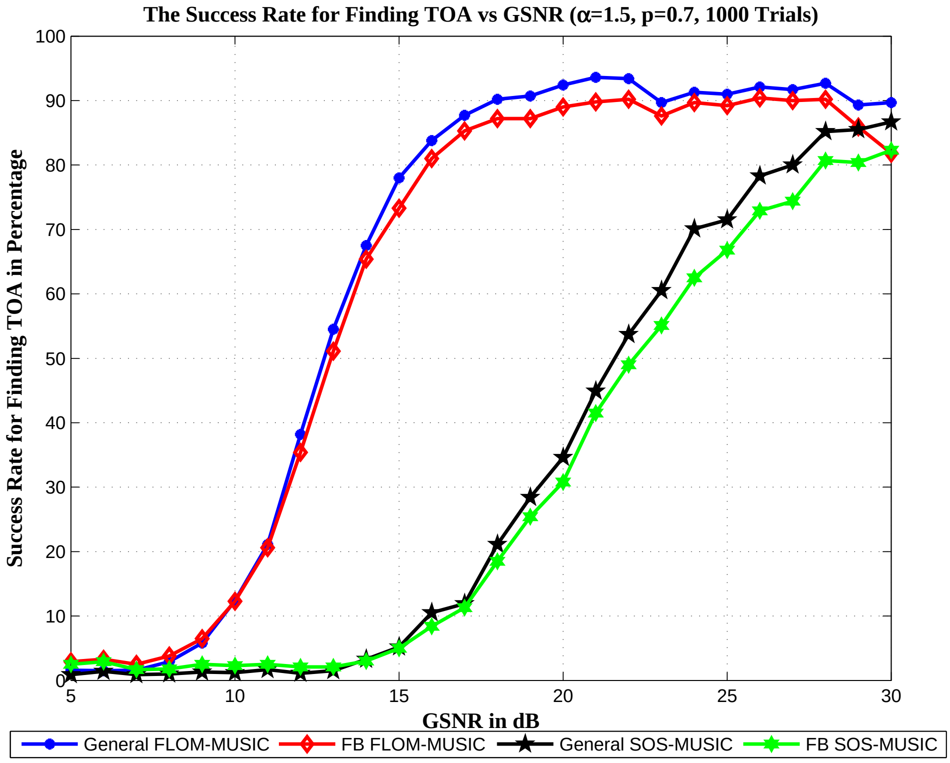

Figure 5.12. Success rate for finding TOA vs GSNR for $\alpha = 1.5$ and $p = 0.7$

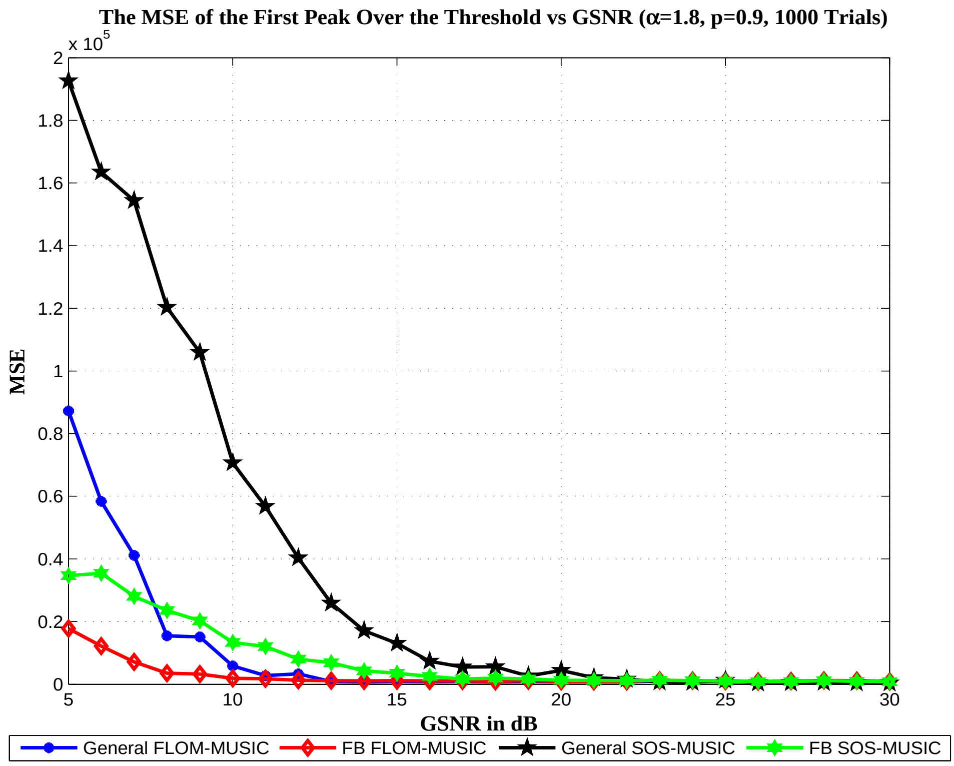

Figure 5.13. MSE vs GSNR for $\alpha = 1.8$ and $p = 0.9$

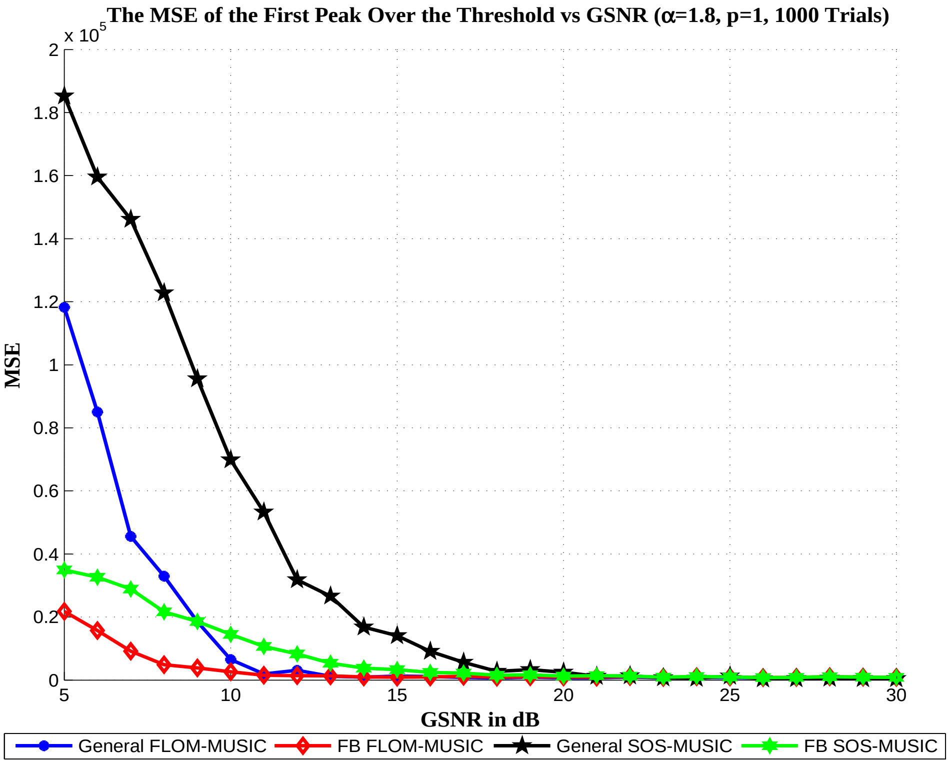

Figure 5.14. MSE vs GSNR for $\alpha = 1.8$ and $p = 1$

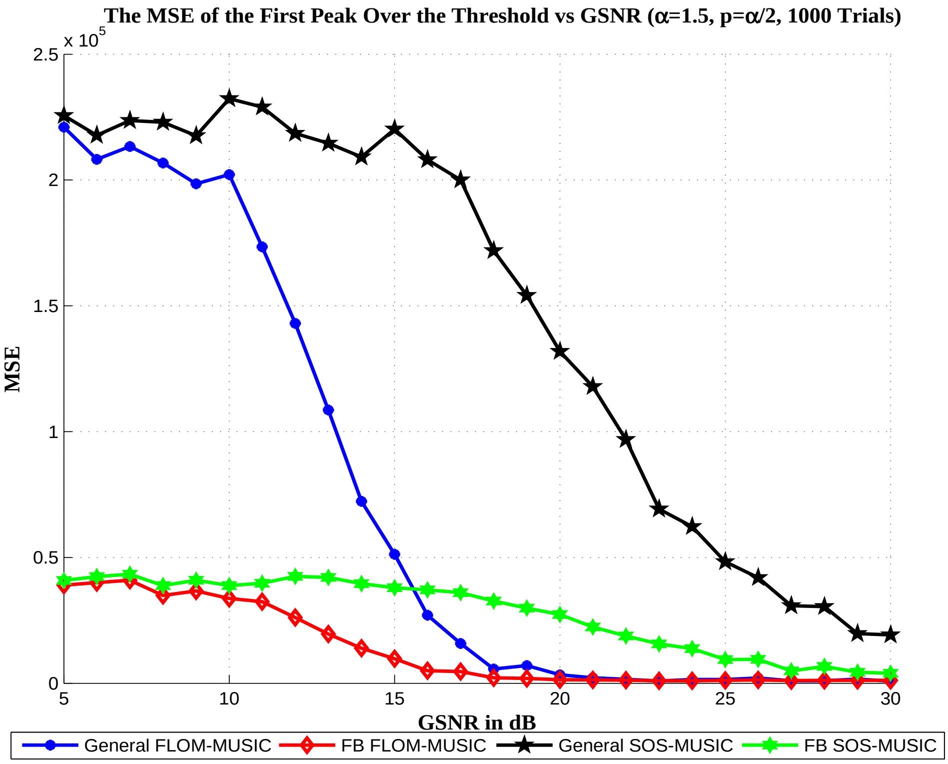

Figure 5.15. MSE vs GSNR for $\alpha = 1.5$ and $p = 0.75$

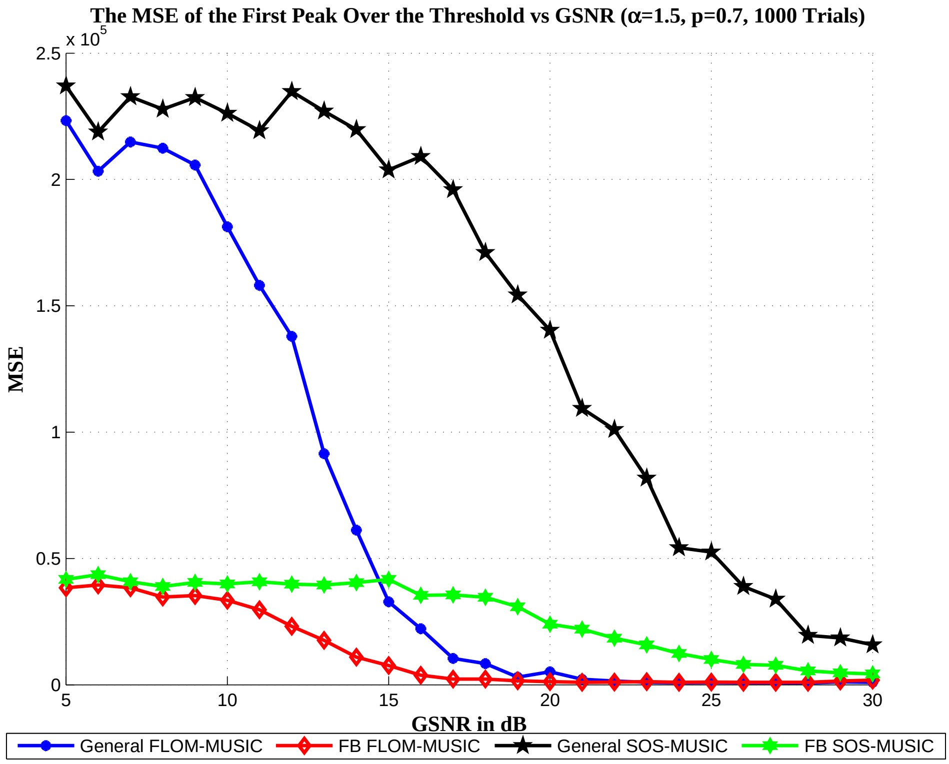

Figure 5.16. MSE vs GSNR for $\alpha = 1.5$ and $p = 0.7$

5.2. The Effect of the Characteristic Exponent α on the Performances of FLOM-MUSIC and SOS-MUSIC

In this section, in order to show the effect of the characteristic exponent α on the performances of estimators, various simulation results are presented. α is changed over [1,2] and 1000 trials were done for (GSNR=25 dB, p=0.7), (GSNR=25 dB, p=1), (GSNR=25 dB, p=$\alpha/2$), and (GSNR=20 dB, p=$\alpha/2$).

In Figure 5.17, Figure 5.18, Figure 5.19, the resolution success rate results for various values of p are presented. As α gets larger than 1.1, a fast increase in the resolution success rates of the general and forward-backward FLOM-MUSIC estimators happens whereas SOS-MUSIC estimators still have poor resolution success rates. As α approaches to the Gaussianity, the performances of the general FLOM-MUSIC and the general SOS-MUSIC TOA estimators get similar. Also the latter resolves two paths slightly better than the former when $\alpha > 1.6$ due to the high GSNR value. As seen from Figure 5.20, in the case of a lower GSNR value (GSNR=20 dB), the general

SOS-MUSIC outperforms the general FLOM-MUSIC after $\alpha > 1,7$. The effect of the fractional moment order on the FLOM-MUSIC estimator and the superiority of the general improvement over the forward-backward improvement are apparent from the figures as well.

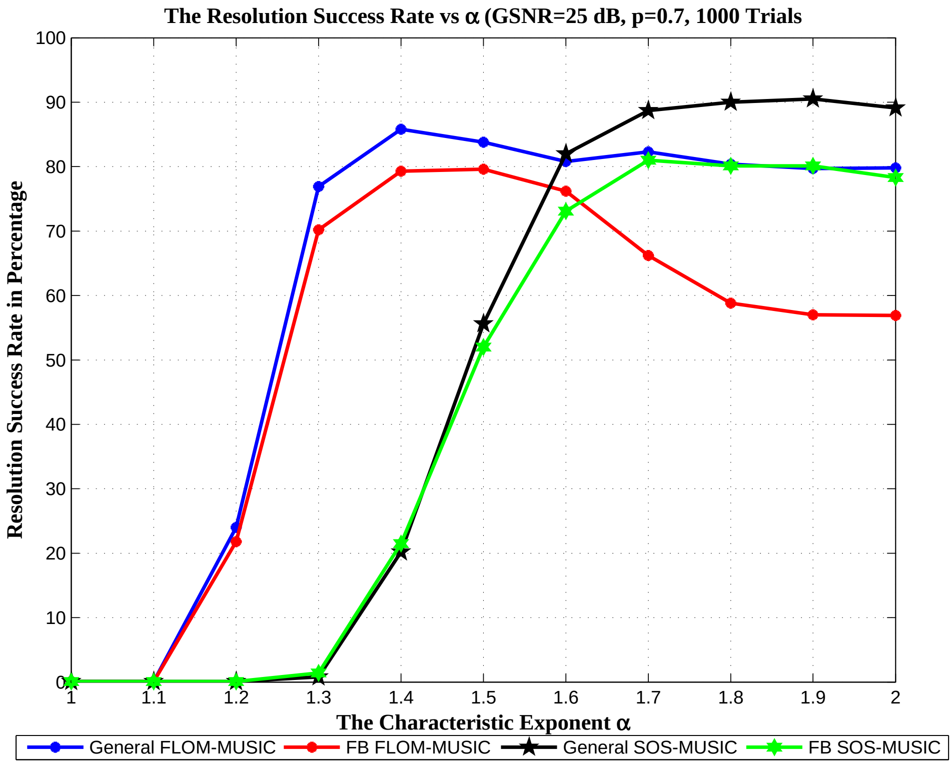

Figure 5.17. The Resolution Success Rate vs α for GSNR=25 dB, p=0.7

Regardless of resolving two paths successfully, Figure 5.21, Figure 5.22, Figure 5.23 and Figure 5.24 present the results of the simulations inspecting the first peak of the pseudospectrum. The same story given for the resolution success rate is valid here. On the other hand, those success rate values are slightly higher than the resolution success rates. Lastly, Figure 5.25, Figure 5.26, Figure 5.27, and Figure 5.28 presents the results of the estimation errors. As seen from the figures, the estimators with forward-backward improvement have lower MSE for low α values, however, as α increases, the general FLOM-MUSIC and SOS-MUSIC show better performance in terms of estimation error. The general FLOM-MUSIC TOA estimator has the lowest MSE for $\alpha > 1.4$. Also the effect of the fractional moment order p is apparent from the figures. In the following section, its effect is investigated via simulation results.

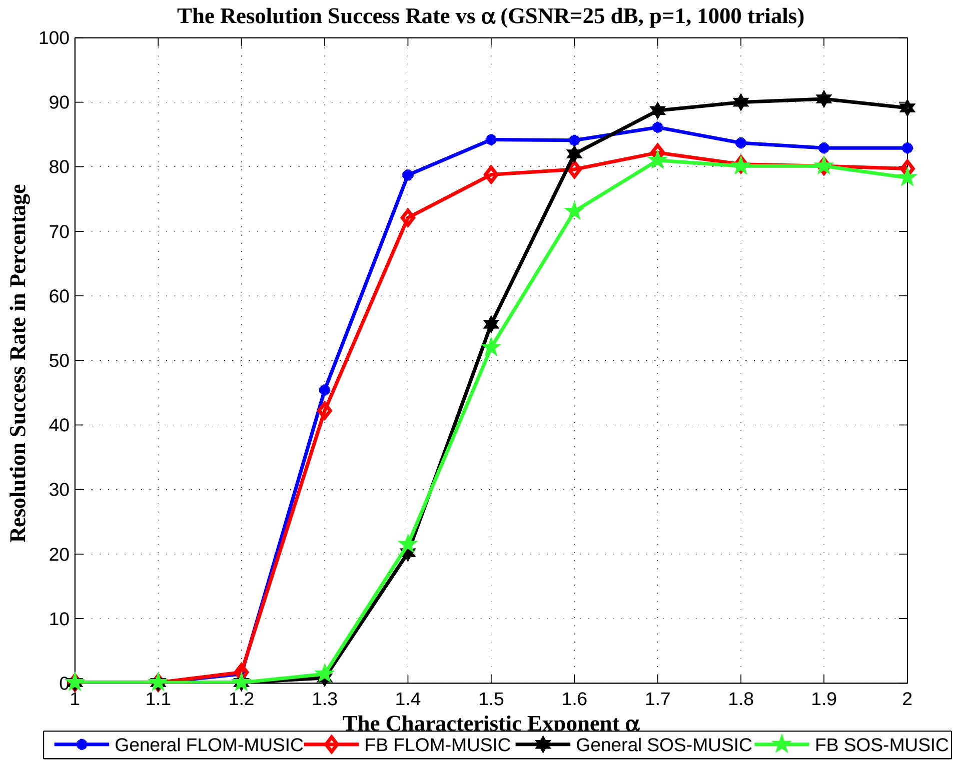

Figure 5.18. The Resolution Success Rate vs α for GSNR=25 dB, p=1

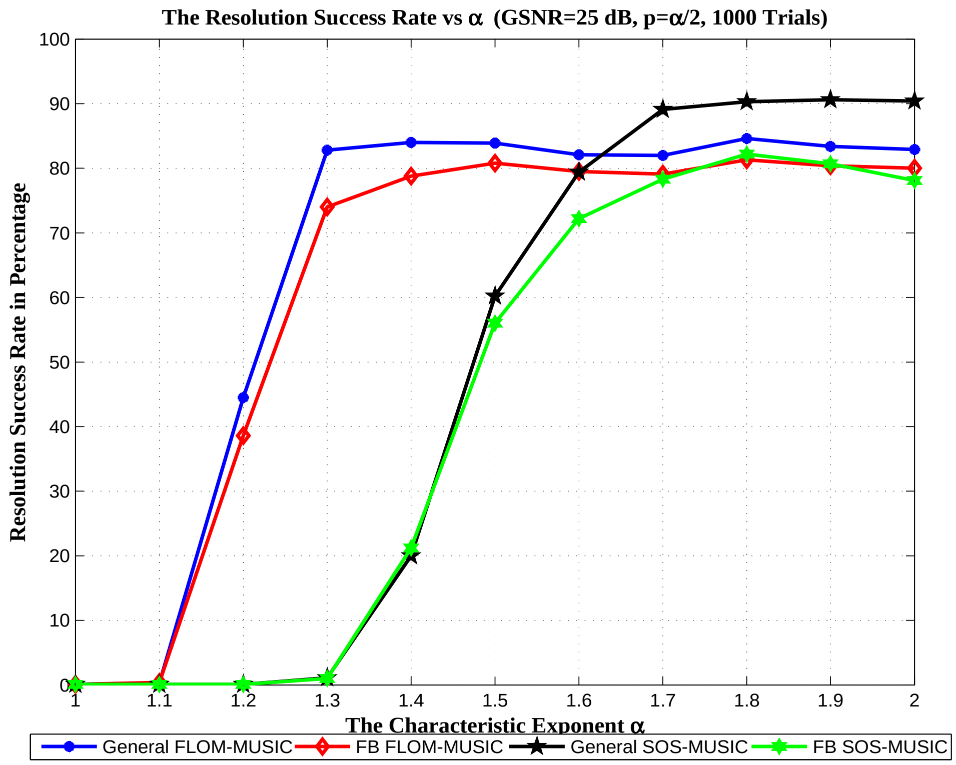

Figure 5.19. The Resolution Success Rate vs α for GSNR=25 dB, $p = \alpha/2$

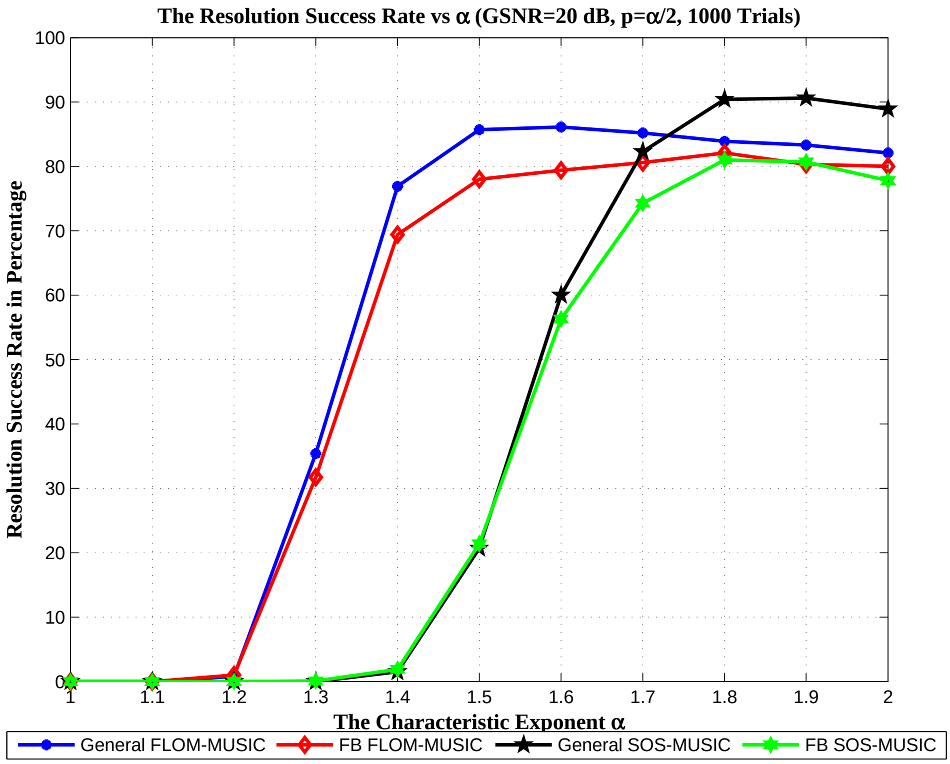

Figure 5.20. The Resolution Success Rate vs α for GSNR=20 dB, $p = \alpha/2$

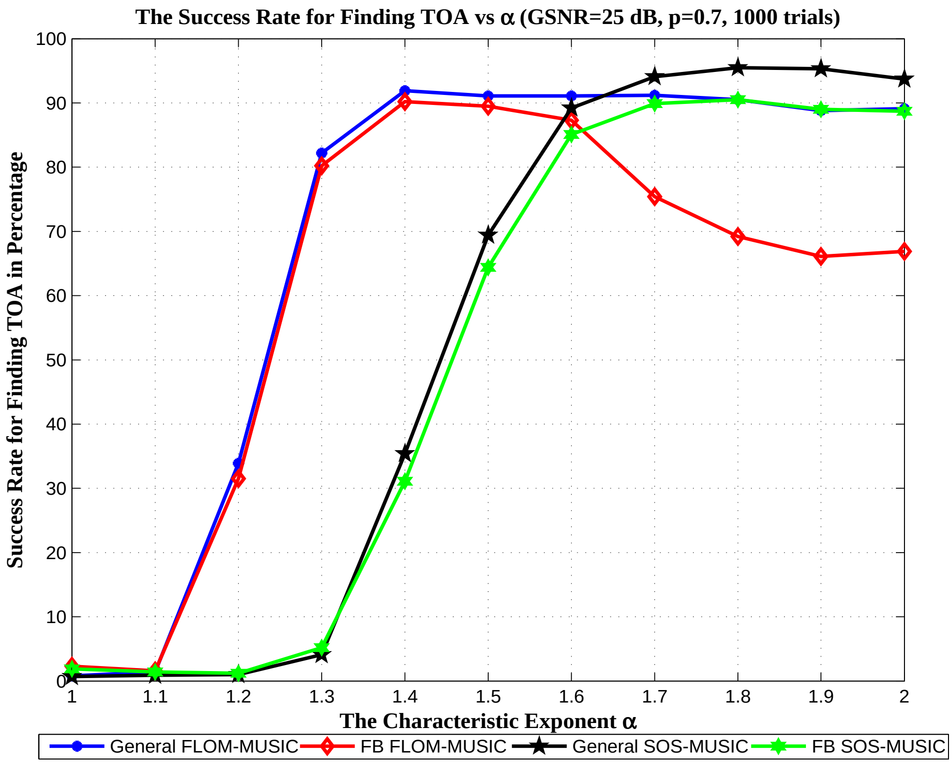

Figure 5.21. The Success Rate for Finding TOA vs α for GSNR=25 dB, p=0.7

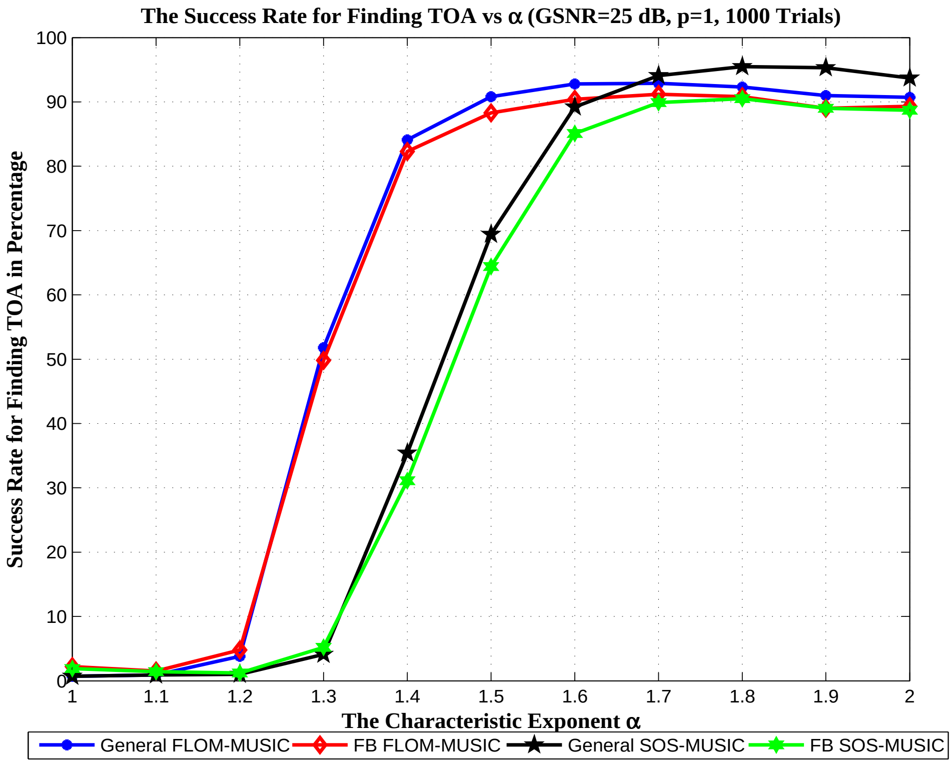

Figure 5.22. The Success Rate for Finding TOA vs α for GSNR=25 dB, p=1

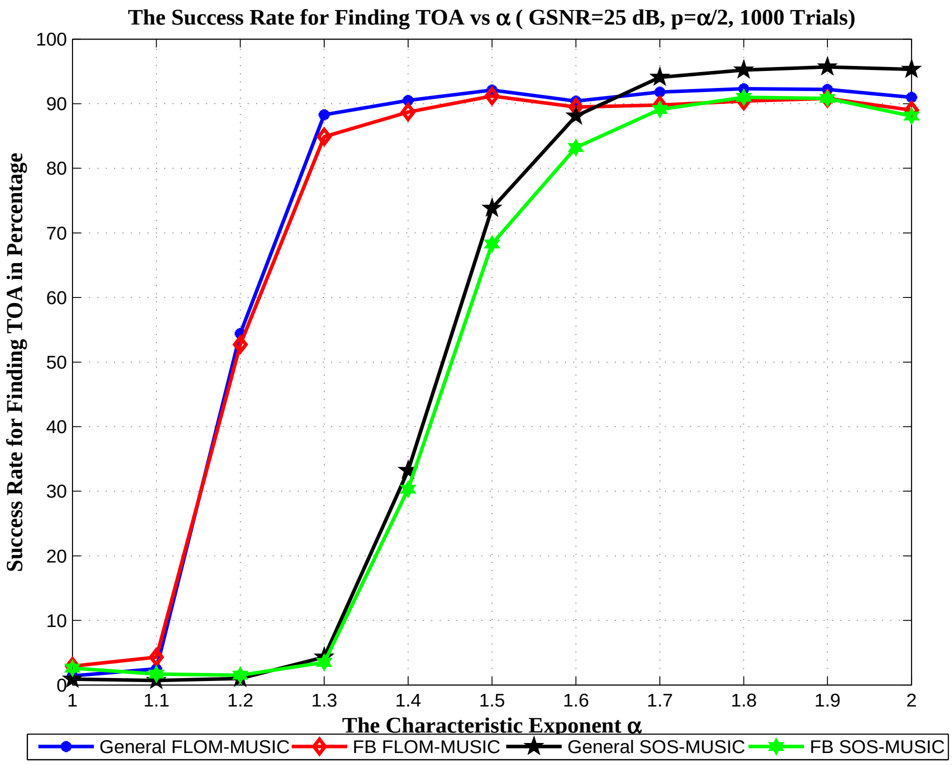

Figure 5.23. The Success Rate for Finding TOA vs α for GSNR=25 dB, $p = \alpha/2$

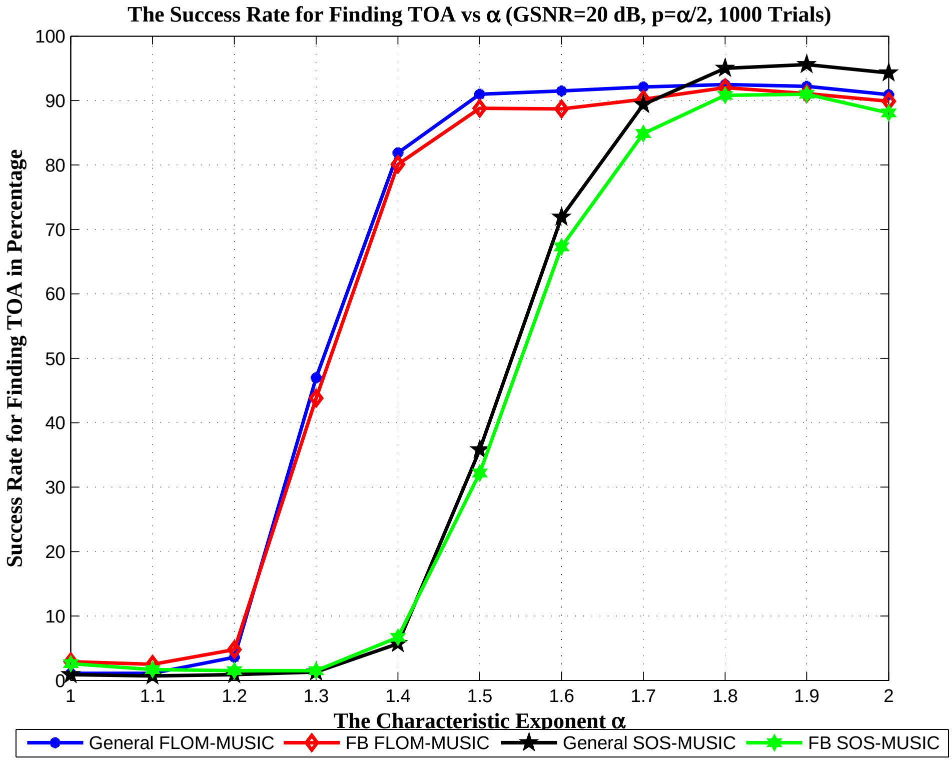

Figure 5.24. The Success Rate for Finding TOA vs α for GSNR=20 dB, $p = \alpha/2$

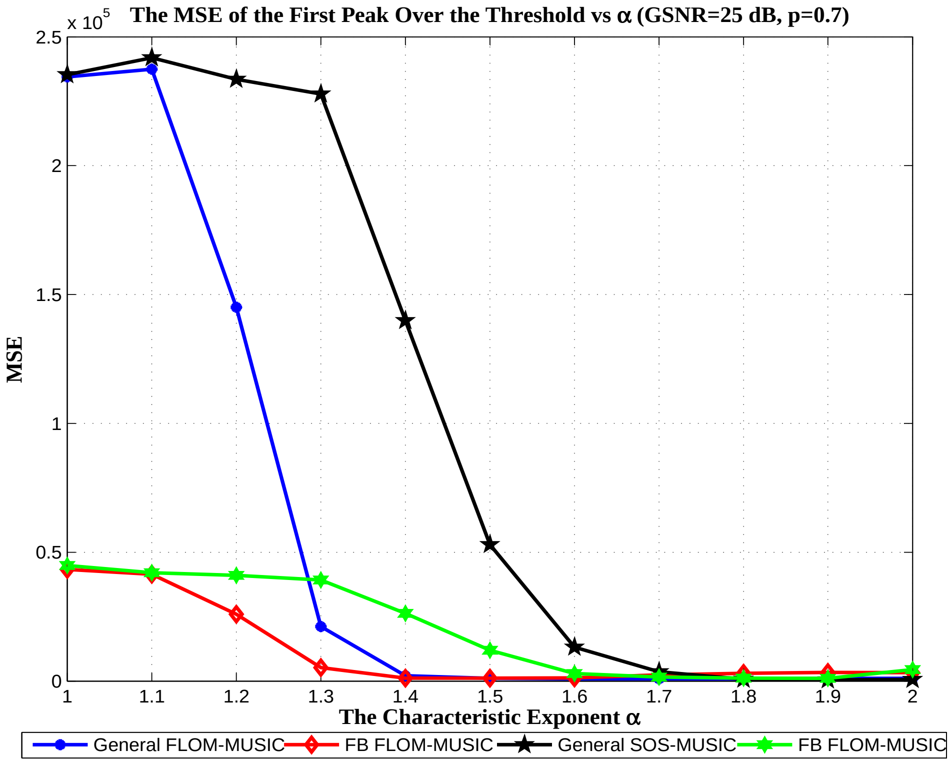

Figure 5.25. MSE vs α for GSNR=25 dB, p=0.7

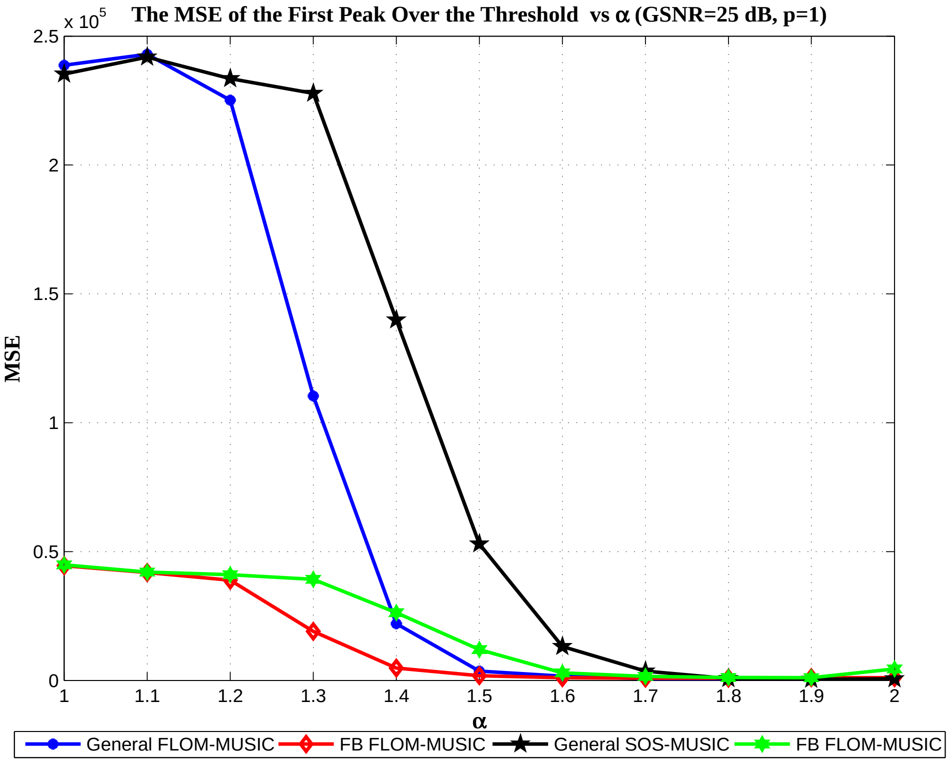

Figure 5.26. MSE vs α for GSNR=25 dB, p=1

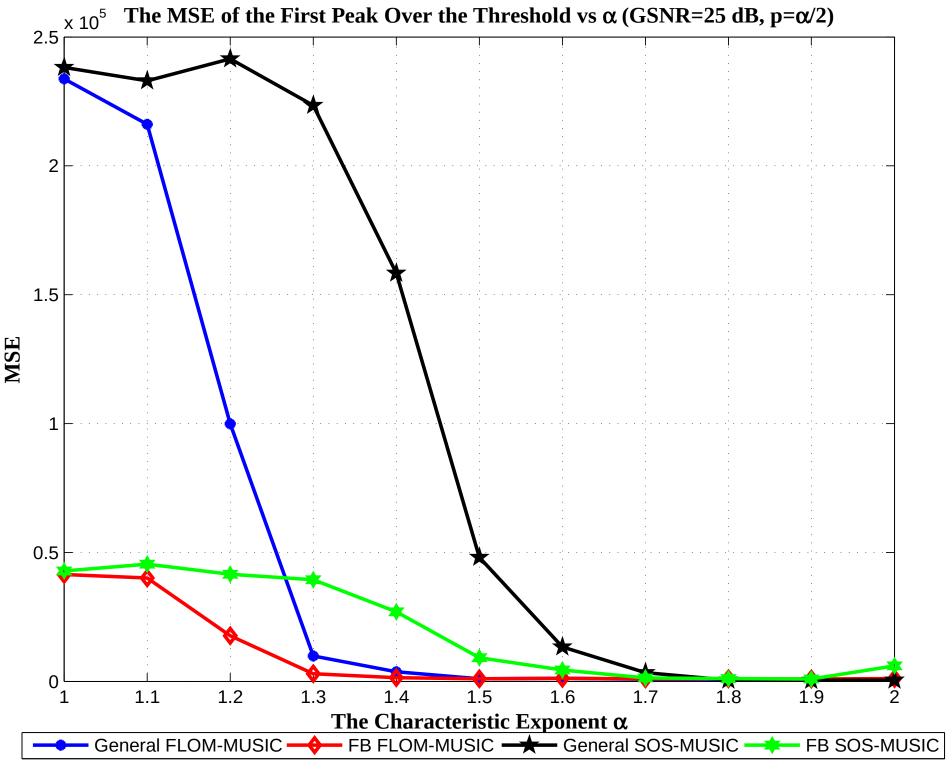

Figure 5.27. MSE vs α for GSNR=25 dB, $p = \alpha/2$

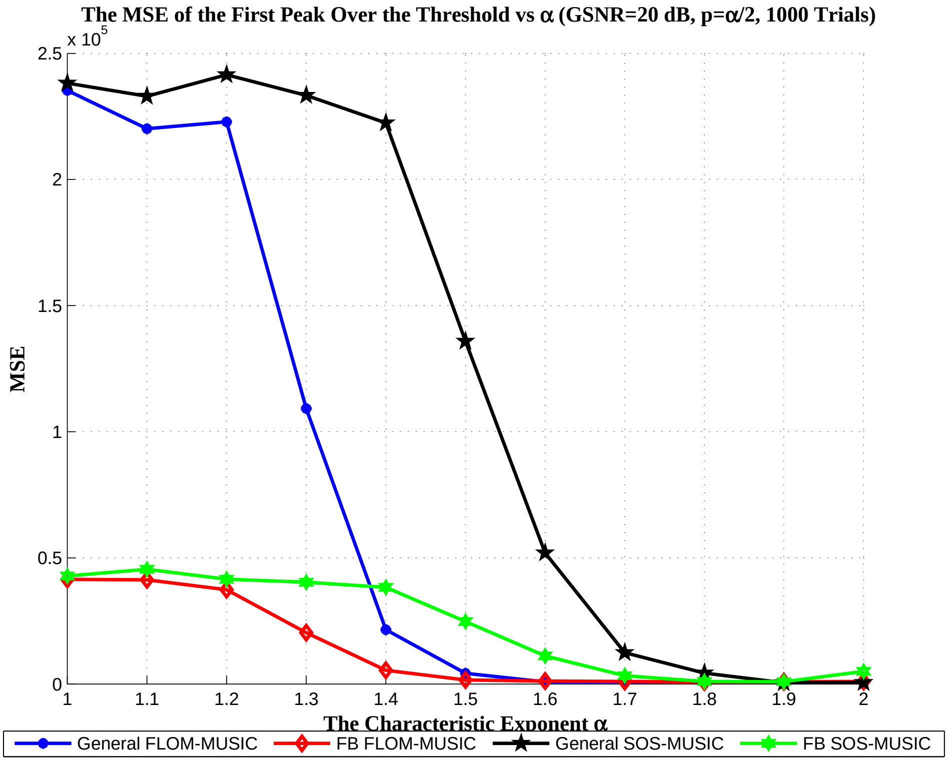

Figure 5.28. MSE vs α for GSNR=20 dB, $p = \alpha/2$

5.3. The Effect of the Fractional Moment Order p on the Performance of FLOM-MUSIC

In this section, simulations are done to see the effect of the fractional lower moment order p on the performances of the estimators. The SOS-MUSIC estimator is independent of p, therefore the general and forward-backward FLOM-MUSIC TOA estimators are compared.

In Figure 5.29, Figure 5.30, and Figure 5.31, the simulation results for GSNR=25 dB and $\alpha = 1.5$ are presented. The effect of the fractional moment order p on the success and the accuracy of both estimators under highly impulsive environment ($\alpha = 1.5$) is apparent. As p increases, the successes of the estimators sharply decrease whereas their MSEs significantly increase. The general FLOM-MUSIC performs better than the forward-backward FLOM-MUSIC in terms of both success rate and MSE. Furthermore, in order to attain higher success rate and lower estimation error, p should be close $\alpha/2$ for highly impulsive environments. Increasing p leads to unsatisfactory performance in terms of both success rate and MSE. For slightly impulsive environments

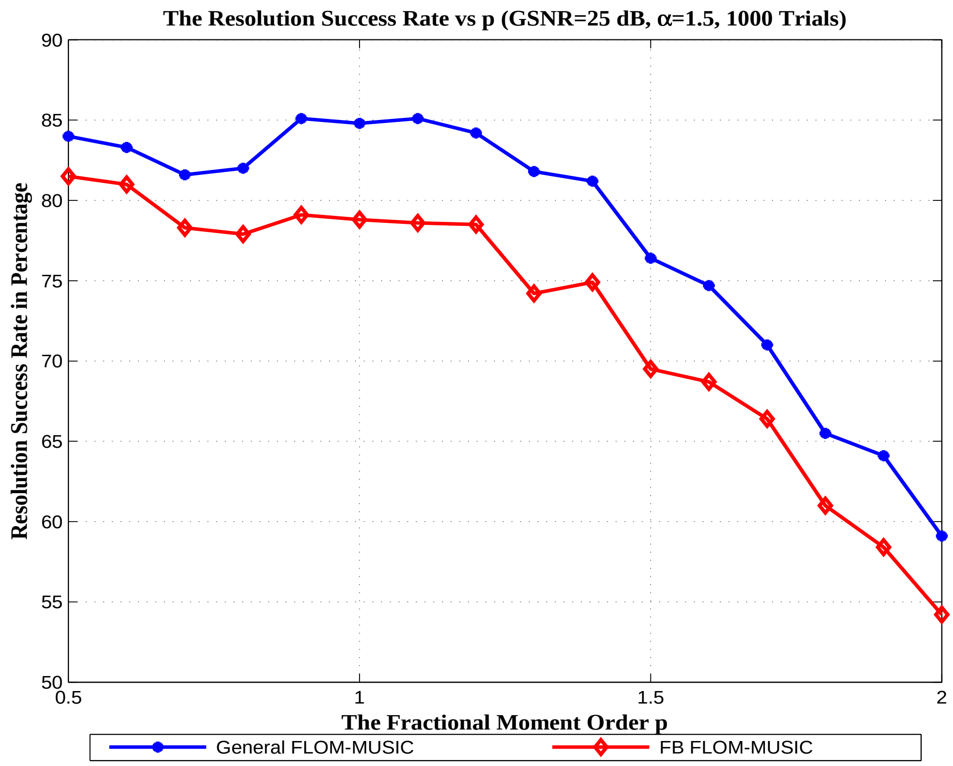

Figure 5.29. The Resolution Success Rate vs p for GSNR=25 dB, $\alpha = 1.5$

($\alpha = 1.8$), simulation results are depicted in Figure 5.32, Figure 5.33, and Figure 5.34. As p approaches to $\alpha/2 = 0.9$, the success rates of the estimators steadily increase while their MSEs sharply decrease. On the other hand, increase in p causes to slight improvement in the success rates. Again, the general FLOM-MUSIC performs better than the forward-backward FLOM-MUSIC.

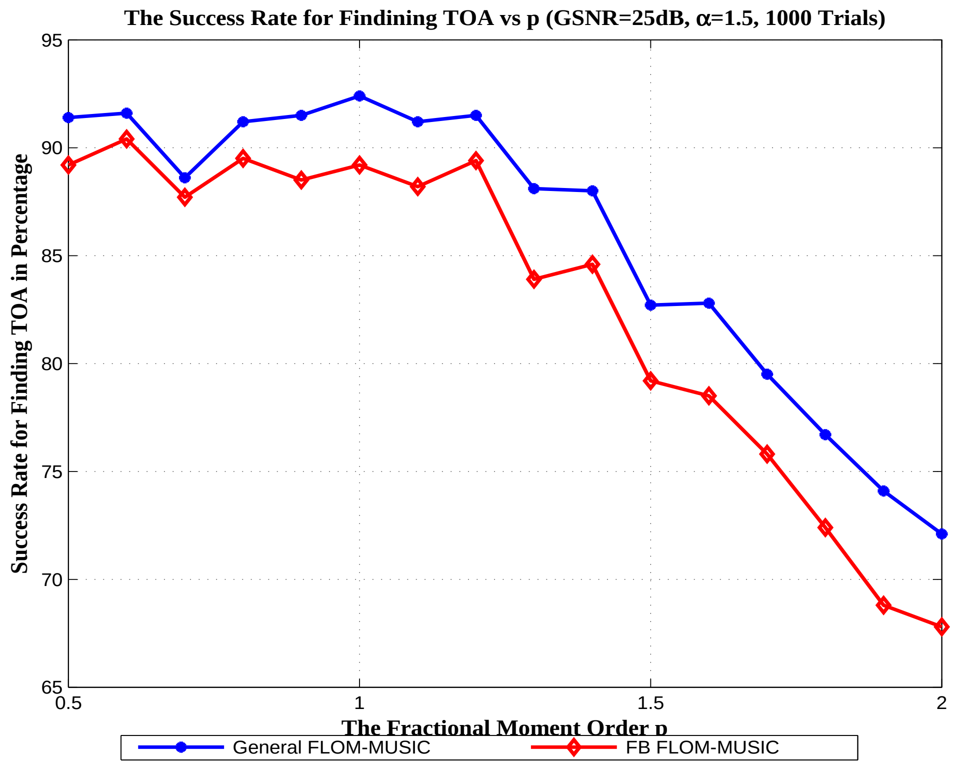

Figure 5.30. The Success Rate for Finding TOA vs p for GSNR=25 dB, $\alpha = 1.5$

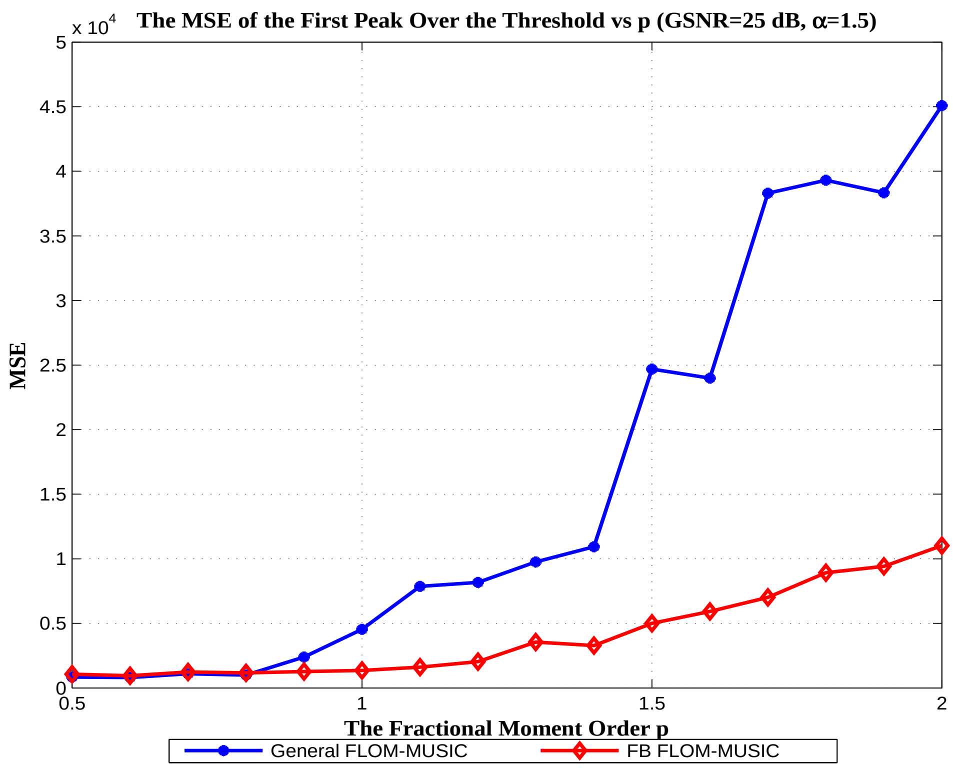

Figure 5.31. MSE vs p for GSNR=25 dB, $\alpha = 1.5$

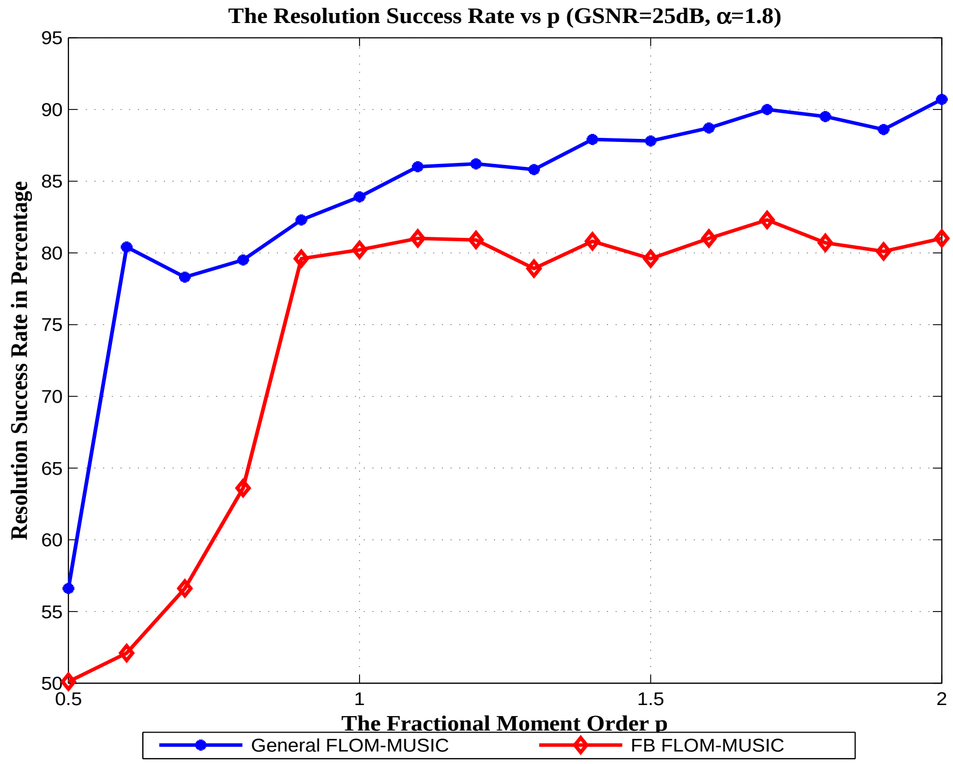

Figure 5.32. The Resolution Success Rate vs p for GSNR=25 dB, $\alpha = 1.8$

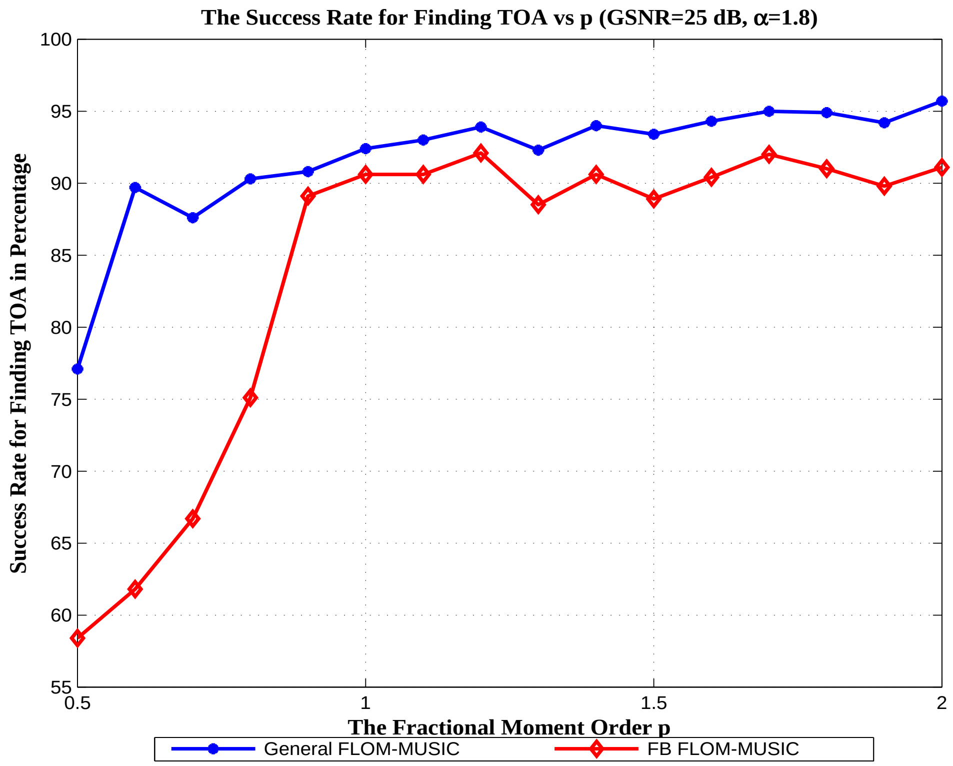

Figure 5.33. The Success Rate for Finding TOA vs p for GSNR=25 dB, $\alpha = 1.8$

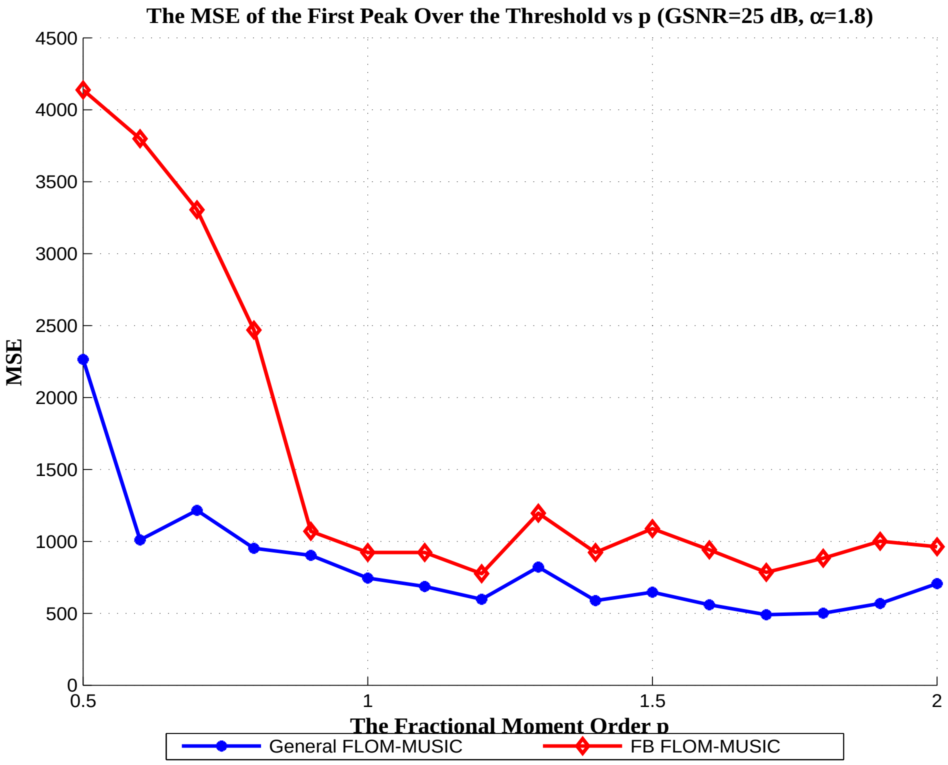

Figure 5.34. MSE vs p for GSNR=25 dB, $\alpha = 1.8$

5.4. The Asymptotical Distribution Tests for FLOM-MUSIC and SOS-MUSIC Estimators

In the literature, the asymptotical distribution of the traditional MUSIC estimator has been studied and under Gaussian noise, in [11] it is shown that SOS-based MUSIC is Gauss-distributed. However, the assumption of impulsive noise changes the distribution. It is not trivial to statistically analyze the distribution of FLOM-MUSIC TOA estimator due to the stable distribution of environmental noise. There are some statistical goodness-of-fit tests in which the validity of one hypothesis is tested without specification of an alternative hypothesis. The Kolmogorov-Smirnov test (KS-test) is such a method that tries to determine if there is a significant difference between two data sets [1]. The advantage of KS-test is that no assumption has to be made about the distribution of data. In other words, it is non-parametric.

First of all, 35000 estimates from the general and forward-backward FLOM-MUSIC and SOS-MUSIC TOA estimators are generated under GSNR=25 dB, α=1.5, and p=0.75. The first peak of the pseudospectrum over the threshold level is evaluated as the estimate.

In Figure 5.35, Figure 5.36, Figure 5.37, and Figure 5.38, the histograms of the four estimators are given. Kolmogorov-Smirnov test is applied to 35000 samples of the

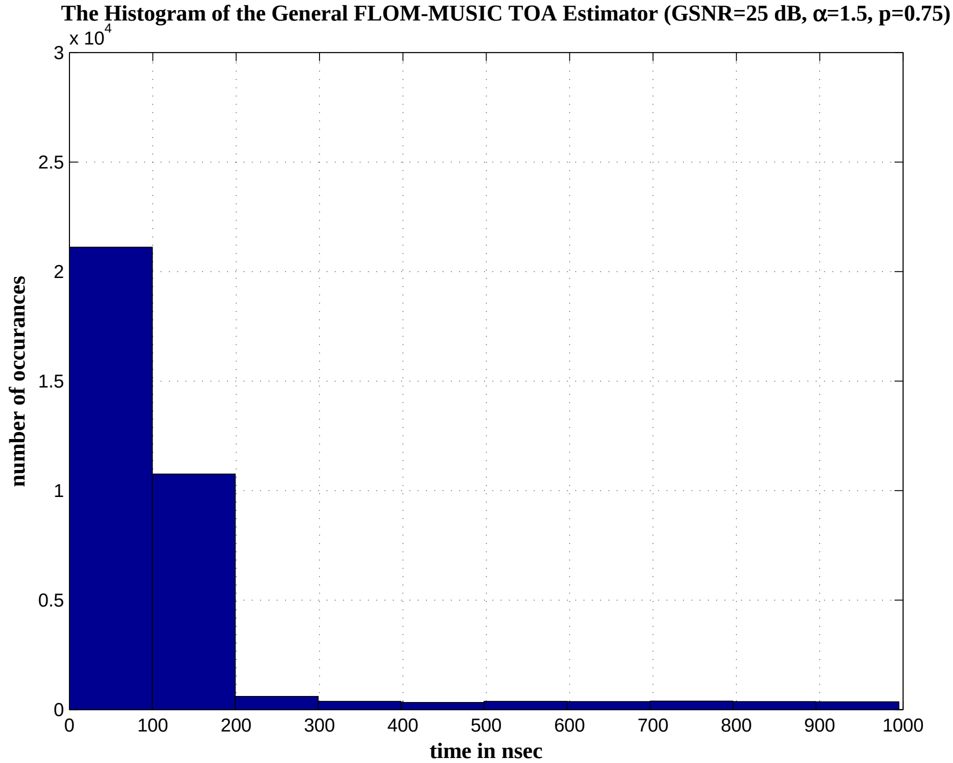

Figure 5.35. The histogram of the general FLOM-MUSIC TOA estimator

general and the forward-backward FLOM-MUSIC and SOS-MUSIC estimators. The normal distribution hypothesis test was rejected at a significance level of 5 per cent, that is, FLOM-MUSIC and SOS-MUSIC TOA estimators do not fit normal distribution. This result can be seen from the figures as well.

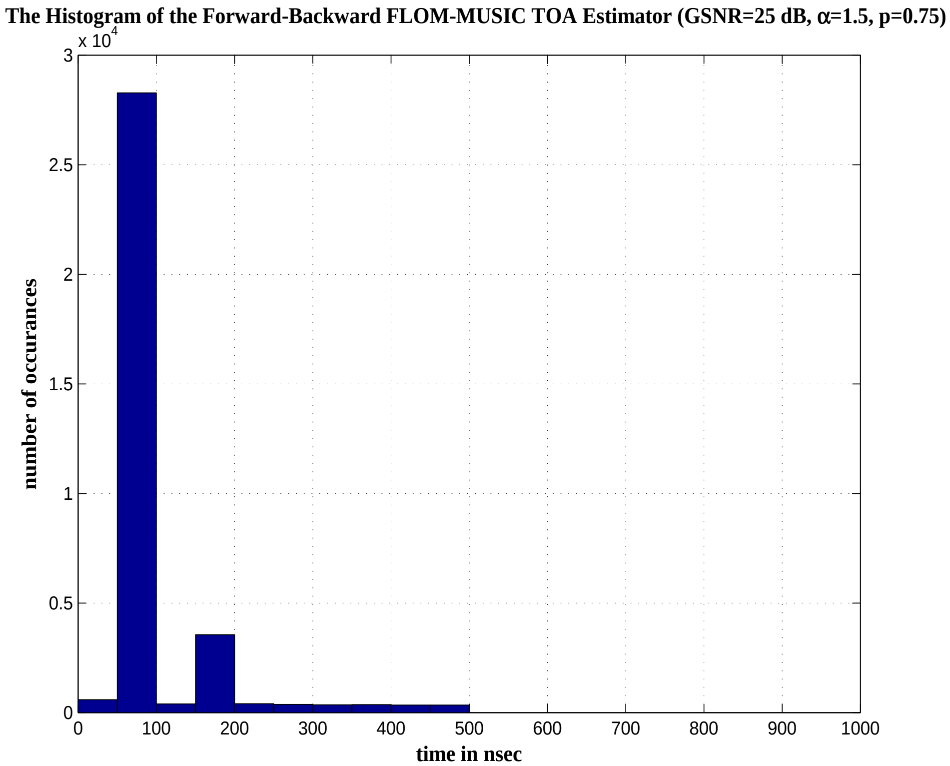

Figure 5.36. The histogram of the forward-backward FLOM-MUSIC TOA estimator

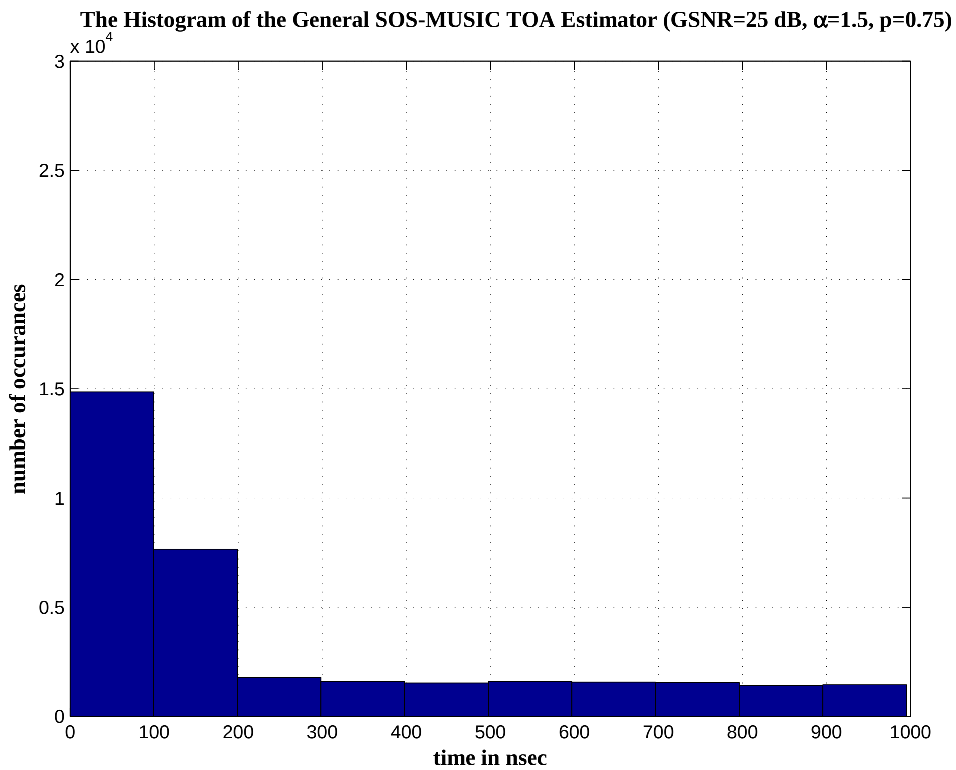

Figure 5.37. The histogram of the general SOS-MUSIC TOA estimator

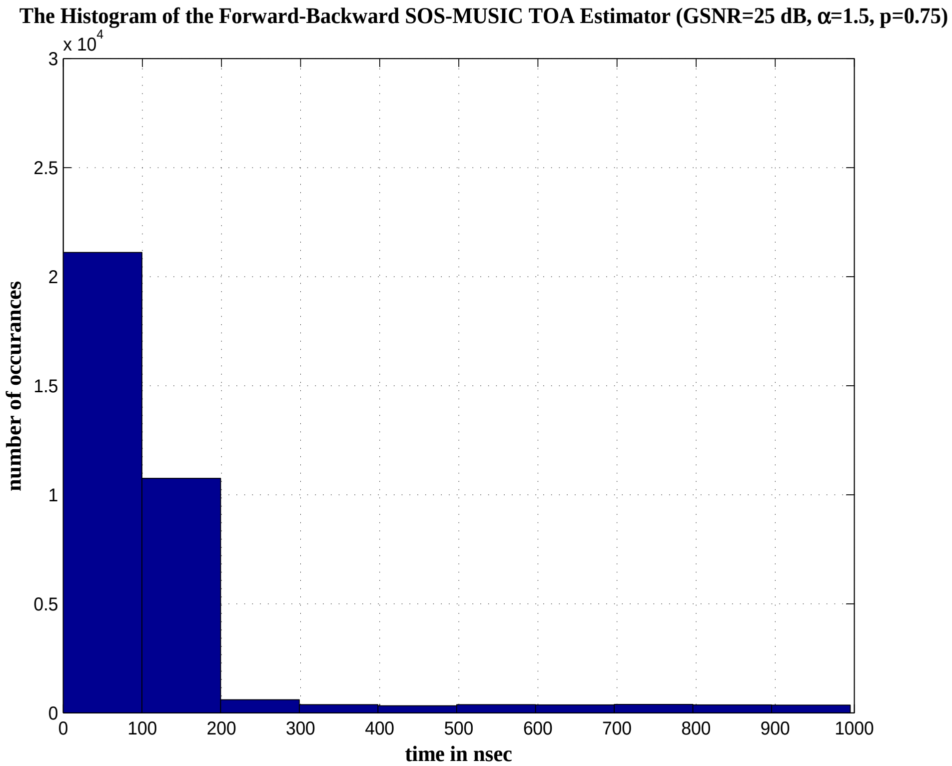

Figure 5.38. The histogram of the forward-backward SOS-MUSIC TOA estimator

6. CONCLUSION AND FUTURE WORK

In this thesis, the TOA estimation with MUSIC under impulsive noise and complex Gaussian multipath indoor channel assumptions is formulated. The environmental noise is assumed to be $S\alpha S$ distributed. The structure of the FLOM-based covariation matrix is similar to the structure of the second-order based covariance matrix proposed in [16]. The MUSIC is applied to the FLOM-based covariation matrix, and the delay of the first arriving path, TOA, is estimated. Also two improvement methods, namely, general and forward-backward, are applied to the covariation matrix in order to obtain Hermitian symmetry.

Simulations are run for the evaluation of the performance of the proposed estimator. Also, the SOS-MUSIC is applied to the problem in order to see the difference between the FLOM-MUSIC and the SOS-MUSIC TOA estimators under impulsive noise.

Two criteria are defined as the evaluation parameters; the success rate and the MSE. Simulation results show that the proposed FLOM-MUSIC outperforms the traditional SOS-MUSIC in terms of both parameters.

In this study, it is shown that the SOS-MUSIC TOA estimator fails under low GSNR values. On the other hand, our simulation results show that the proposed FLOM-MUSIC TOA estimator have satisfactory performance under this circumstance in terms of resolution capability and low estimation error. Furthermore, it is seen that the general FLOM-MUSIC works better than the forward-backward FLOM-MUSIC.

The effect of the characteristic exponent α on the performances of the estimators are investigated via simulations. Under low α values, the SOS-MUSIC gives completely poor results whereas the FLOM-MUSIC works well.

Due to the fact that the FLOM-based covariation matrix depends on the fractional moment order p, the performances of the general and the forward-backward FLOM-MUSIC TOA estimators with respect to p are studied. Our simulation results show that the value of p significantly affects the performance of the estimator and the optimum p value is close to $\alpha/2$ especially for low characteristic exponent values. As α approaches to 2 which is the Gaussian case, it can be chosen larger than $\alpha/2$.

Finally, the Kolmogorov-Smirnov test is applied to 35000 samples of the general and the forward-backward FLOM-MUSIC and SOS-MUSIC estimators. It is seen that these estimators do not fit the Gaussian distribution. The obtained histograms of the estimators support this result as well.

All in all, in this thesis, it has been shown that TOA estimation under impulsive noise can be done by applying the FLOM-MUSIC while the SOS-MUSIC cannot be used. Especially for low GSNR values and under highly impulsive environments where α is around 1.5, it apparently outperforms SOS-MUSIC. Another useful result stemming from this study is that the fractional moment order p should be chosen carefully because it affects the success of the FLOM-MUSIC TOA estimator. A wrong choice may lead to high estimation errors. Our simulation results show that p should be around $\alpha/2$ for $\alpha \in [1, 1.5]$ whereas it is possible to increase p as the distribution of noise approaches to Gaussian. Lastly, it is not trivial to define the statistical distribution and bounds of the estimator. The future work will focus on the asymptotical distribution and error bound of FLOM-MUSIC TOA estimator.

REFERENCES

1. *Kolmogorov-Smirnov Test,* http://www.physics.csbsju.edu/stats/KS-test.html.

2. A. Papoulis, *Probability, Random Variables and Stochastic Processes.* McGraw-Hill, 1984.

3. C. L. Nikias and M. Shao, *Signal Processing with Alpha-Stable Distributions and Applications.* Wiley-Interscience, New York 1995.

4. G. Morrison and M. Fattouche, "Super-Resolution Modeling of the Indoor Radio Propagation Channel," *IEEE Transactions on Vehicular Technology*, vol. 47, no. 2, pp. 649–657, May 1998.

5. H. Amindavar and A. M. Reza, "A New Simultaneous Estimation of Directions of Arrival and Channel Parameters in a Multipath Environment," *IEEE Transactions on Signal Processing*, vol. 53, no. 2, pp. 471–483, February 2005.

6. H. Hashemi, "The Indoor Radio Propagation Channel," *Proceedings of the IEEE*, vol. 81, no. 7, pp. 943–968, July 1993.

7. K. Pahlavan and P. Krishnamurthy, *Principles of Wireless Networks:A Unified Approach.* Prentice Hall, 2002.

8. M. A. Altınkaya, H. Deliç, B. Sankur and E. Anarım, "Subspace-Based Frequency Estimation of Sinusoidal Signals in Alpha-Stable Noise," *Signal Processing*, vol. 82, pp. 1807–1827, 2002.

9. N. A. Alsindi, *Performance of TOA Estimation Algorithms in Different Indoor Multipath Conditions.* MSc Thesis, Worcester Polytechnic Institute, 2004.

10. N. Patwari, A. O. Hero, M. Perkins, N. S. Correal and R. J. O'Dea, "Relative Location Estimation in Wireless Sensor Networks," *IEEE Transactions on Signal*

Processing, vol. 51, no. 8, pp. 2137–2148, August 2003.

11. P. Stoica and T. Söderström, "Statistical Analysis of MUSIC and Subspace Rotation Estimates of Sinusoidal Frequencies," *IEEE Transactions on Acoustics, Speech and Signal Processing*, vol. 339, no. 8, pp. 1836–1847, August 1991.

12. P. Tsakalides, *Array Signal Processing with Alpha-Stable Distributions.* PhD Thesis, University of Southern California, 1995.

13. P. Tsakalides and C. L. Nikias, "The Robust Covariation-Based MUSIC (ROC-MUSIC) Algorithm for Bearing Estimation in Impulsive Noise Environments," *IEEE Transactions on Signal Processing*, vol. 44, no. 7, pp. 1623–1633, July 1996.

14. T. H. Liu and J. M. Mendel, "A Subspace-Based Direction Finding Algorithm Using Fractional Lower Order Statistics," *IEEE Transactions on Signal Processing*, vol. 49, no. 8, pp. 1605–1613, August 2001.

15. T. S. Rappaport, *Wireless Communications:Principles and Practice.* Prentice Hall, Englewood Cliffs, NJ, 1996.

16. X. Li and K. Pahlavan, "Super-Resolution TOA Estimation with Diversity for Indoor Geolocation," *IEEE Transactions on Wireless Communications*, vol. 3, no. 1, pp. 224–234, January 2004.

17. H. Zaghloul, G. Morrison, and M. Fattouche, "Frequency response and path loss measurements of indoor channel," *IEE Electronics Letters*, vol. 27, no. 12, pp. 1021–1022, June 1991.